Design and Development of a Bio-inspired Robotic Jellyfish that Features Ionic Polymer Metal Composites Actuators

Joseph Samih Najem

Thesis submitted to the Faculty of the
Virginia Polythechnic Institute and State University
in partial fulfillment of the requirements for the degree of

Master of Science
in
Mechanical Engineering

Donald J. Leo, Chair
Daniel J. Inman
Shashank Priya
Stephen A. Sarles

April 27, 2012
Blacksburg, Virginia

Design and Development of a Bio-inspired Robotic Jellyfish that Features Ionic Polymer Metal Composites Actuators

Joseph Samih Najem
Virginia Polythechnic Institute and State University
Donald J. Leo, Advisor

ABSTRACT

This thesis presents the design and development of a novel biomimetic jellyfish robot that features ionic polymer metal composite actuators. The shape and swimming style of this underwater vehicle are based on oblate jellyfish species, which are known for their high locomotive efficiency. Ionic polymer metal composites (IPMC) are used as actuators in order to contract the bell and thus propel the jellyfish robot. This research focuses on translating the evolutionary successes of the natural species into a jellyfish robot that mimics the geometry, the swimming style, and the bell deformation cycle of the natural species. Key advantages of using IPMC actuators over other forms of smart material include their ability to exhibit high strain response due to a low voltage input and their ability to act as artificial muscles in water environment. This research specifically seeks to implement IPMC actuators in a biomimetic design and overcome two main limitations of these actuators: slow response rate and the material low blocking force. The approach presented in this document is based on a combination of two main methods, first by optimizing the performance of the IPMC actuators and second by optimizing the design to fit the properties of the actuators by studying various oblate species.

Ionic polymer metal composites consist of a semi-permeable membrane bounded by two conductive, high surface area electrode. The IPMCs are manufactured is several variations using the Direct Assembly Process (DAP), where the electrode architecture is controlled to optimize the strain and stiffness of the actuators. The resulting optimized actuators demonstrate peak to peak strains of 0.8 % in air and 0.7 % in water across a frequency range

of 0.1-1.0 Hz and voltage amplitude of 2 V.

A study of different oblate species is conducted in order to attain a model system that best fits the properties of the IPMC actuators. The *Aequorea victoria* is chosen based on its bell morphology and kinematic properties that match the mechanical properties of the IPMC actuators. This medusa is characterized by it low swimming frequency, small bell deformation during the contraction phase, and high Froude efficiency. The bell morphology and kinematics of the *Aequorea victoria* are studied through the computation of the radius of curvature and thus the strain energy stored in the during the contraction phase. The results demonstrate that the *Aequorea victoria* stores lower strain energy compared to the other candidate species during the contraction phase.

Three consecutive jellyfish robots have been built for this research project. The first generation served as a proof of concept and swam vertically at a speed of 2.2 mm/s and consumed 3.2 W of power. The second generation mimicked the geometry and swimming style of the *Aurelia aurita*. By tailoring the applied voltage waveform and the flexibility of the bell, the robot swam at an average speed of 1.5 mm/s and consumed 3.5 W of power. The third and final generation mimicked the morphology, swimming behavior, and bell kinematics of the *Aequorea victoria*. The resulting robot, swam at an average speed of 0.77 mm/s and consumed 0.7 W of power when four actuators are used while it achieved 1.5 mm/s and 1.1 W of power consumption when eight actuators are used.

Key parameter including the type of the waveform, the geometry of the bell, and position and size of the IPMC actuators are identified. These parameters can be hit later in order to further optimize the design of an IPMC based jellyfish robot.

To my parents,

Samih and Najat,

my only brother Mario,

my sister and brother-in-law Nancy and Robert,

and my best friend Yara

Acknowledgments

Many people have greatly contributed to the work presented in this thesis[1]. I would like to thank Dr. Donald Leo for his wise guidance and continuous encouragement. Dr. Andy Sarles and Dr. Barbar Akle both deserve special recognition for their friendship, support, and always having perfect answers to my questions. I would also like to thank Dr. Daniel Inman and Dr. Shashank Priya for their insights and recommendations that has benefited this achievement. I would also like to express gratitude to Beth Howell for her helpful assistance. Additionally, my CIMSS colleagues, both former and present, all deserve special thanks for their friendship, technical advice, and willingness to lend a hand. Last but not least, I would like to acknowledge my family who have supported me from the start. I am blessed for my parents, sister, brother, and my best friend Yara for their love, support, and patience.

<div align="right">

JOSEPH NAJEM

</div>

Virginia Polytechnic Institute and State University

27th April 2012

Contents

List of Figures

List of Tables

Chapter 1

Introduction

The interest in developing underwater vehicles that mimic jellyfish especially for their high locomotive efficiency and simple design [1], has arisen with the recent demand for novel types of autonomous underwater vehicles. This type of bio-mimetic robot has been extensively studied, developed, and characterized in the Center for Intelligent Material Systems and Smart Structures (CIMSS) lab at Virginia Tech [2, 3, 4]. Different aspects of the jellyfish robot were studied, ranging from propulsion and actuation to energy harvesting, sensor implementation, and communication.

Various propulsion and actuation mechanisms were explored at CIMSS. The actuation mechanisms adapted, were mainly based on smart materials such as: shape memory alloys (SMA) and ionic polymer metal composites (IPMC) [2, 3, 4]. This thesis will focus on the design of a bio-inspired jellyfish robot that features ionic polymer metal composites (IPMC) actuators. This robot mimics the geometry, morphology, and swimming style of the natural jellyfish species. The following chapters will relate to the fabrication and characterization of the IPMC actuators, bell kinematics properties of different jellyfish species, and the design,

fabrication, and characterization of the robot.

1.1   Problem Statement

Autonomous underwater vehicles (AUVs) are robots able to travel underwater or swim without any human intervention. AUVs are valuably used in monitoring animals, humans, and environmental changes; to name a few: seafloor survey and mapping for oil and gas detection on the commercial level [5]. AUVs are also extensively used for military application such as detecting mines and/or manned submarines, as well as monitoring protected areas for unidentified objects [6]. Scientists also use AUVs for the study of ocean floor and animal migration, the detection of chemical agents, and the preserve of microscopic life [5].

Because current technologies suffer from practical limitations, the uses of AUVs have been forced to be limited to a certain number of tasks [5]. Examples of these restraints include: significant maintenance requirement, cost-effectiveness, lifetime and range [6]. However, the main problems associated with existing AUVs can be summarized by the following: first, most AUVs used today are powered by rechargeable batteries which limit their range of operation and have limited lifetime [7]. Larger vehicles use aluminum based semi-fuel cells batteries that require substantial maintenance and thus high cost of operation; moreover they produce waste products that might disturb the ocean life thus harming the environment. Second, most common propulsion techniques are propeller based thrusters or kort nozzles. These thrusters are commonly powered by electric motors that usually require special sealing techniques [8]. This process of waterproofing is usually impacted by the decision of brushed or brushless motors, which lastly affects the reliability, efficiency, and the cost [9].

Recent demand for autonomous underwater vehicles, such as robotic fish and even au-

tonomous alligators, for use in military and commercial applications motivates the design and development of new types of self-propelling, bio-inspired crafts. Two requirements for a successful vehicle design include the ability to demonstrate proficient swimming and maneuverability in order to maintain position in water, and provide long-term, efficient use of the available energy stored on-board [10, 11]. To this point, interest in developing underwater vehicles that mimic jellyfish is based on their high locomotive efficiency, ability to survive in different water and environmental condition, and relatively simple and convenient design to carrying payload [12, 13, 14].

New forms of propulsion and actuation have been also investigated for this purpose. These techniques are based on bio-inspired materials that can serve as artificial muscles that in turns can help mimicking the structure, morphology and swimming behavior of the natural animal [4, 3, 2, 15]. Initial attempts to build robotic jellyfish have used either shape memory alloys (SMAs) or ionic polymer metal composites for providing actuation to a synthetic bell structure.

1.2   Literature Review

In this section, brief background information on AUVs and ionic polymer metal composites will be provided. The review has started with the definition of AUVs in addition to a list of existing ones and their applications with the emphasis on bio-mimetic designs. Next, since we are mainly interested in the actuation and propulsion aspect of the design, historical background on common actuation and propulsion mechanisms is provided and followed by a brief overview on the use of smart material and electro-active materials as actuators in such vehicles. Finally, the ionic polymer metal composites properties, manufacturing methods and present applications is explored and discussed.

1.2.1   Unmanned Underwater Vehicles

Unmanned underwater vehicles usually fall under two categories, the Remotely Operated Vehicles (ROVs) and the Autonomous Underwater Vehicles (AUVs) [6]. ROVs are usually physically connected, through a tether that provides both power and control, to a controller that can be either on a submarine or a ship. In contrast, AUVs are completely autonomous and depend in most cases on an onboard power system or controller [6].

The motivation of building and developing underwater vehicles is not recent. In 1775 at Saybrook, Connecticut, David and Ezra Bushnell built the first American submarine which they called "Turtle". The Turtle was later used in New York Harbor in 1776, in the first naval battle in history involving a submarine [16].

"Resurgam" the world's first practical submarine was built in November of 1879 by the Reverend George W. Garrett. This vehicle was powered by a Lamm 'fireless' steam engine, and was able to travel for around ten hours counting on the power stored in an insulated tank [17].

Many more underwater vehicles have been developed after the aforementioned historic vehicles for numerous different tasks. Subsequently, torpedoes the first AUVs were developed even though many AUV systems were studied prior the 1970s. Since the beginning of the 1970s a great and valuable amount of development occurred [17].

Actually, the development of AUV began in the 1960s, where some vehicles were built and mainly served in very specialized cases specifically data gathering [16]. On the other hand, during the 1970s a respectful amount of initial attempts and experimental prototypes were built. For instance, the UARS and SPURV vehicles were developed by the University of Washington APL [18]. These vehicles were mainly used in data gathering. The Marine

Systems Engineering Laboratory (University of New Hampshire) has developed the EAVE vehicle. In parallel, the Institute of Marine Technology Problems (Russian Academy of Sciences) started their research on AUVs and developed the SKAT vehicles along with the L1 & L2 known to be the first deep diving AUVs. The seventies period is known as the time of experimentation in order to define the potential of developing AUVs [6].

During the 1980s several proof of concept prototypes were built and fully characterized as the result of the major advances in technology that occurred at that time. As a result to these successes the first "International Symposium on Unmanned Untethered Submersible Technology" (UUST) was held and took place in Durham, New Hampshire, USA [7]. Many people from both the industry and the universities attended. The eighties period represented an important turning point for AUV technology, and was culminated by launching several research programs in the USA which provided funding for the development of proof of concepts prototypes.

During the 1990s, the AUVs grew from proof of concepts into initial generation that served as operational systems able to perform specific tasks. However, the first truly commercial products did not become available until year 2000. In this decade the utilization of AUV systems for many commercial and military applications has became obvious. Around 145 different types of AUV were developed and are available in the market nowadays. However, there are still many technological obstacles that has to be overcome[17].

1.2.2 Biomimetic Unmanned Underwater Vehicles

The design and development of biomimetic underwater vehicles have been recently the focus of major research efforts. The goal of this cutting-edge field is to translate the evolutionary successes of natural species into artificial systems that mimic the construction, function, and

performance of the living systems [10, 11].

At the beginning of year 2008, the development of bio-inspired underwater vehicles that mimic the designs found in nature, started. Most of the attempts are still in their experimental stages, and they were able to exhibit high propulsion efficiency and maneuverability when compared to the traditional results.

In 2008, Festo a well known German industrial control and automation company, has developed the first biomimetic jellyfish robot called *"AquaJelly"*. This robot is a self-controlling system that mimics the swimming behavior if the natural jellyfish. It consists of a translucent hemisphere and eight tentacles for propulsion [18]. A central electric motor powered by two lithium-ion polymer batteries, is placed at the center of the robot and is responsible of the propulsion. In 2009, a biomimetic robot that mimics the "Manta" fish was developed by Evologics which is another German company that focuses on developing innovative key technologies for aerospace, maritime, and offshore industries [8].

Bio-inspired underwater vehicles, has been the research interest for many research groups around the world. Many robots mimicking different kinds of marine species have been. At Virginia Tech different research groups are studying the capability to mimic jellyfish through a MURI project funding by the Office of Naval Research.

1.2.3 Actuation Mechanisms/Smart Materials

Most Autonomous Underwater Vehicles are based on motors for locomotion. These common propulsion techniques used nowadays, are mainly propeller based. The propeller based robots are either thrusters or Kort nozzles, which are powered by electric motors. These techniques are usually associated with low efficiency, reliability, and high cost of operation

and maintenance.

For the past couple years the research has been focused on finding more efficient and maneuverable means of propulsion. This will lead to increase the duration of the mission and the generally efficiency and performance of the vehicle. People started to look at nature in order to create new ways of thinking in engineering designs. This is achieved by using the biological systems to improve the engineering technology.

The new technologies in biology, active materials, and robotics fields, help realizing the biomimetic propulsion and fish-like swimming robots [10]. These types are usually known by "biologically inspired underwater vehicle" (BIUV), and usually obtain thrust by imitating the swimming behavior of fishes.

Therefore, new forms of propulsion and actuation have been investigated for this purpose. These techniques are based on bio-inspired materials that can serve as artificial muscles that in turn can help mimic the structure, morphology and swimming behavior of the natural animal.

Initial attempts to build robotic jellyfish have used either shape memory alloys (SMAs) [2]. Villanueva, et al demonstrated the fabrication of a jellyfish robot that utilized eight SMA actuators for propulsion [2]. While Villanueva, et al was able to closely mimic the swimming motion and speed of the natural jellyfish (Aurelia aurita), the main disadvantage of a SMA-powered jellyfish is the high power consumption required to actuate the SMA materials. The RoboJelly consumed an average and peak power of 14W and 80W, respectively [2].

Ionic Polymer Metal Composites (IPMCs) are a type of electroactive material that produces mechanical deformation in response to an applied electrical field [19]. As shown in Figure 1, the IPMC, or more specifically the semi-permeable membrane, will bend toward the anode

upon application of an electric field. This is caused by the motion of the mobile cations within the polymer matrix [20]. As a result, IPMCs are often thought of as artificial muscles and may enable a lighter weight, lower-power alternative to Shape Memory Alloys (SMA) materials for actuating a robotic jellyfish.

In 2009, Yeom et al [15] published their results about a biomimetic jellyfish robot that is based on IPMC actuators. The paper discusses the design, fabrication and characterization of the robot. The robot did not swim freely, however a floating controller was used to maintain neutral buoyancy. Results about velocity were presented, the maximum achieved vehicle speed of 0.057 mm/s, but data on power consumption were not presented.

1.2.4   Historical Background on Ionic Polymers and their Application

Ionic polymer metal composites (IPMCs) are type of electroactive materials that exhibit large deformation in response to a low applied voltage [19]. This process is reversible where a dynamic deformation of an IPMC can produce a dynamic electric field across the electrodes [21]. IPMCs showed a huge potential to act as soft robotic actuators, artificial muscles, and electro-dynamic sensors.

An IPMC consists of an ionomeric semi-permeable membrane sandwiched by two conductive electrodes [21]. The metal electrodes are meant to increase the intensity of the electric field applied to the membrane during actuation. The metal or metal particles are deposited on the membrane, in a way to maximize the interfacial area between the membrane and the metal electrode. In order to get better performance the electrical resistance of the electrode has to be minimized. There are usually two types of electroding techniques: chemical and

mechanical. Usually chemical techniques are more expensive and time consuming, however they provide better adhesion. In contrast, mechanical techniques are adapted due to the ability to deposit non-precious metals on the membrane for instance Ruthenium dioxide and Carbon nanotubes. The major disadvantage of this method is inability of this material to function well in hydrated mediums [22].

Chemical electroding methods usually consist of reducing the metal particles stored in the membrane with the assistance of reducing agents [22]. This method has been the subject of interest for many research groups that focused on improving and developing techniques of chemical metal deposition. The mechanical electroding techniques are mainly based on three different techniques: physical vapor deposition, solution casting, and the direct assembly process[22].

Historical, polymer-metal were developed as early as the 1930's [23]. However, at the beginning of 1990's their sensing ability was reported by Sadeghipour, et al. In 1992 Oguro's group in Japan discovered the bending ability of the ionic polymers due to an applied potential across the thickness of the membrane [23]. Since that moment, several groups across the world worked and are still working on improving the manufacturing process, in order to improve the actuation capacity and search for applications for this new material.

Ionic polymers materials have many interesting properties that make of them special kind of smart materials. These materials are usually large displacement low force actuators [24]. They are soft compared to the brittle ceramics electroactive polymers and have complaint structures. Many applications need large displacement actuators, and here were the ionic polymers come into the picture. Moreover, the ionic polymer metal composites are biocompatible especially the Nafion based ones which makes them potential muscle implants.

The interesting properties of IPMCs listed earlier give them a number of potential applica-

tions. These applications range from their application as sensors to actuators. They can be used in different environments, in water submerged applications, and in different forms i.e. packaged polymers or ionic liquid diluent based polymers (Bennett and Leo, 2004).

IPMC have been used in industrial and biomedical applications for instance biomimetic robotic sensors, actuators, and transducers. An IPMC can be used as a mechanical gripper on both micro and macro levels, in this application two IPMC actuators are placed in parallel with top faces facing each other. To date multi-finger grippers have been produced, these grippers consist of two, four, and eight fingers. IPMCs have also been used as three-dimensional actuators, robotic swimming structure, and Linear actuators.

On the medical level IPMCs have been used as Metering valves, Diaphragm pumps using flexing IPMC strips and diaphragms, and Exo-skeletal human joint power augmentation. On the micro level MEMS and microrobots made with IPMCs represent and enabling technology for manufacturing sensor and actuator microarrays in addition to several other applications.IPMCs have also found application in the Biomedical field for example Artificial ventricular or cardiac-assist muscles, Surgical tool, and Peristaltic pumps.

In conclusion these materials can provide an efficient method to convert mechanical energy into electrical or chemical forms and thus work as sensors in addition to their capability of being used as actuators. This section presents a summary of the efforts on a number of potential applications of ionic polymer metal composites.

1.3 Different Jellyfish Species Morphology and Swimming Behavior

In this section a study on different jellyfish species is presented. Understanding the morphology and swimming behavior of the species is important in order to achieve a biomimetic robotic jellyfish design. On the other hand, as mentioned in the previous section IPMC materials are soft and have slow response rate. This study will help in attaining a jellyfish species that fits the mechanical and electrical properties of the IPMC actuators. The geometry and bell kinematics is first discussed followed by the propulsion types and efficiency of different medusae. In the second part the swimming behavior of different oblate species is discussed and finally a summary including the important properties and key factors related to jellyfish shape and swimming style.

1.3.1 Jellyfish Types: Oblate vs. Prolate Species

Jellyfish species are usually classified under two main categories: prolate and oblate species [12]. This classification is directly related to the geometrical shape of the jellyfish's bell. Prolates are characterized by their elongated bell shape with a fineness ratio larger than 1.0. In contrast, oblate species have a more flattened shape with a fineness ratio less than 0.5. The fineness ratio is a number used by the biologists in order to characterize the jellyfish swimming behavior [25] and is defined as the ratio of the bell height to its diameter,

$$F = h/d. \tag{1.1}$$

Biologists proved that the swimming style and efficiency of jellyfish species are highly correlated with the bell geometry [14, 26]. Oblates depend on a starting and a stopping vortices caused by the non-uniform deformation of the bell, in order to propel themselves. The bell of an oblate species minimally contracts at the top while the maximum contractions are located toward the margin which causes the starting and stopping vortices. These vortices are represent a critical part of the rowing propulsion technique adapted by the oblates during the swimming cycle [14].

Rowing propulsion is characterized by a slow and non-uniform bell contractions compared to the jetting technique in order to generate forward thrust [14]. The stopping vortex is generated on the interior of the bell during the bell expansion. Directly after the generation of the stopping vortex, the bell contracts and generates the starting vortex along the margin of the bell. This vortex interaction impacts the swimming behavior of the medusa by producing a more efficient mode of swimming even though it is slower.

In contrast, prolate species contract their bell in a uniform fashion causing water jet which will cause the forward propulsion of the jellyfish. A comparison between the oblate and prolate species is shown in Table 1.1. The results demonstrate that the oblates are more efficient even though they swim at a slower speed. Froude efficiency is used to compare the energetic efficiency of the thrust produced by both propulsion techniques for a living organism or a vehicle and is defined as follows,

$$Fr_p = \frac{2V_m}{V_j + V_m} \times 100, \tag{1.2}$$

where V_m is the velocity of the medusa, and V_j is the velocity of the jet. The proficiency on the other hand is defined as the ratio of the velocity V_m to the bell diameter d.

Table 1.1: A comparison between prolate and oblate jellyfish species.

	Prolate	Oblate
Bell contraction	Fast	Slow
Acceleration	High	Low
Froude efficiency	Low	High
Proficiency	High	Low

1.3.2   Swimming Behavior of Different Oblate Species

This section focuses on studying different oblate species since these species proved to be more efficient compared to the prolates. Data for four oblate species are found in literature. The studied species are as follows: *Aurelia aurita, Aequorea victoria, Mictrocoma cellularia, and Phialidium gregarum.* Table 1.2 shows a comparison among these species in terms of physiologically relevant parameters. In this table the fineness ratio ranges are associates with the contracted and relaxed phases respectively. For instance, the *Aequorea victoria* has the smallest range where its fineness ratio ranges from 0.42 (relaxation phase) to 0.55 (contraction phase) as opposed to 0.39 to 0.7 for the *Mictrocoma cellularia.* In addition to the fineness ratio range, another important criteria we looked at is the swimming frequency and it was found that the *Mictrocoma* swims at a low frequency (0.5 Hz) compared to the others, while the *Aequorea victoria* swims at 1.1 Hz. Based on this study the focus is now on the Aequorea victoria as a good candidate since it has the smallest fineness ratio range with the second lowest swimming frequency.

1.3.3   Summary

In summary, the jellyfish species fall under two main categories based on their geometrical shape. The shape of the medusa affect its swimming style and efficiency. The oblate species

Table 1.2: A comparison among four different oblate species in terms of fineness ratio range, swimming frequency, peak accelaration, and peak velocity[14].

	Aequorea victoria	*Aurelia aurita*	*Mictrocoma cellularia*	*Phialidium gregarum*
Fineness ratio range	0.42-0.55	0.39-0.7	0.5-0.7	0.3-0.6
Frequency (Hz)	1.1	0.5	1.67	1.67
Peak acceleration (cm/s^2)	5	5	10	10.2
Peak velocity (cm/s)	2	1.5	2.5	1.3

are more efficient, however slow swimmer and this is due to the rowing propulsion technique adapted by these species. On the other hand, the prolate species are less efficient but swim faster due to the water jetting propulsion technique. Different oblate species are studied and their properties were identified which will help in designing a biomimetic robot. On the other hand this study helps in finding the species that best fits the properties if the IPMC actuators.

1.4   Motivation

The initial focus of this thesis is to study the feasibility of using ionic polymer metal composites as actuation and propulsion mechanisms for a biomimetic jellyfish like underwater vehicle. Initial attempts to build robotic jellyfish have used shape memory alloys (SMAs). Villanueva, et al demonstrated the fabrication of a jellyfish robot that utilized eight SMA actuators for propulsion. While Villanueva was able to attain a biomimetic design by closely mimicking the swimming motion and speed of the natural jellyfish, the main disadvantage of a SMA-powered jellyfish is the high power consumption. Therefore, IPMCs were suggested as an alternative espacially that ionic polymers have been used in many different applications due to their interesting properties especially their ability to exhibit large deformation due

to a low applied voltage.

In 2009, Yeom et al published their results about a bomimetic jellyfish robot based on IPMC actuators. The resulting robot achieved a speed of 0.057 mm/s, but no data on power consumption were presented. The major difficulties with ionic polymers was the small force they generate and their slow response rate, thus the focus at the beginning went on improving both properties by optimizing the structure of the electrodes. This attempt was successful but we were faced by the limitations of the material especially at the actuation frequencies we are using. On a different level the focus shifted toward finding a jellyfish specie that better fits the properties of the IPMC actuators. Therefore, the aim of this thesis changed from optimizing the IPMC actuators to both optimizing the material and the design of the whole system by mimicking the species that better fits the mechanical properties of IPMCs.

1.5 Overview of the Thesis

1.5.1 Research Objectives

The objective of this thesis is to design, build, and develop a biomimetic jellyfish robot that uses ionic polymer metal composites actuators. Ionic polymer actuators can achieve high strain deformation (5%) for a low voltage applied (2-5 V). The operation of those actuators depends on the mobility of ions inside the polymer clusters. Therefore, these transducers are know for low response rate. Another interesting property of IPMCs is the small force that they can generate.

The first objective of our research, was to improve the performance of the IPMC actuators, especially building such actuators using the Direct Assembly Process (DAP) is knew and

had never been optimized. The optimization study focuses on the structure and chemical composition of the high surface area electrodes bounding the Nafion^{TM} membrane.

The second objective of our research was to attain a jellyfish species that can serve as a model system and specifically fits the limiting properties of the IPMC actuators. This approach represents a bio-inspired solution of the limiting properties of the actuators. Finally, the goal of this research is to build a biomimetic robot that mimics the geometry, bell kinematics, and swimming style of the natural jellyfish.

1.5.2 Contribution

The main contribution of this research is the development of a novel low power biomimetic jellyfish robot based on IPMC actuators. In order to characterize the free-swimming performance of the robot, the vertical displacement of the robot in water was measured. In addition the power consumption was also measured by recording the voltage and the current consumption during the swimming test.

During the characterization process it was realized that several parameters affect the swimming behavior of the robot. First, the amplitude, frequency, and duty cycle of the input signal to the robot affect dramatically the performance of the robot specifically the swimming speed and the power consumption. Second, mimicking the bell kinematics had a major effect on the power consumption which was reduced due to the reduction in the actuators' sizes. Third, the geometry of the jellyfish bell also affects its behavior where introducing cuts in the bell increased the swimming speed of the robot. Finally, it was noticed that adding flaps at the tip of the margin also improves the performance of the jellyfish robot. Finally, this whole research could evolve into a larger project where each aspect and parameter discussed above can be targeted separately in order to achieve a more robust low power robot.

1.5.3   Approach

Chapter 2 provides an overview for experimental setups and procedures in addition to the characterization tests performed in order to characterize the ionic polymer actuators and the robot.

Chapter 3 is devoted for the fabrication and characterization of the IPMC actuators. In addition some preliminary optimization attempts are discussed. Finally, a summary of the experimental bending and impedance measurements results is presented.

Chapter 4 discusses the bio-inspired bell kinematics design of the jellyfish robot. In the first section, a comparative bell kinematics analysis is conducted between two competitive medusae *Aurelia aurita* and *Aequorea victoria*. In the second section, a discussion of a biomimetic bell kinematics design is presented, and it focuses of the design, characterization, and results of a bio-inspired bell, that mimics the morphology and kinematics of the natural jellyfish.

Chapter 5 presents the design and development of a three different jellyfish robot generations using IPMC actuators for propulsion. The first generation served as a proof of concept, while the second mimicked the *Aurelia aurita*, and the third mimicked the *Aequorea victoria*.

At last, Chapter 6 provides a brief overview of the thesis. It also provides our contribution to the field with conclusions beign drawn.

Chapter 2

Experimental Methods

In this chapter a description of the ionic polymer metal composite actuators, the robotic jellyfish free-swimming, and the bell kinematics design experiments is presented. In addition, the fixtures and circuits used in these experiments will also be discussed. Two experiments are performed in order to characterize the IPMC actuators, electric impedance and free displacement in both water and air. On the other hand, free swimming tests are performed on the jellyfish robot to characterize its performance. These experiments are described in the following sections, with details on the circuitry and equipment used.

2.1   Experiments Outputs

Each experiment, in the IPMC actuators characterization case, is run with a sinusoidal input signal. In the case of free-displacement experiment, this signal is used to actuate the ionic polymer sample. As for the electric impedance measurements, a sinusoidal input voltage is applied and the resulting current flow is recorded.

The outputs of the free-displacement experiment consist of: the input voltage, the current consumption, and the free-tip-displacement. These three sets of data are then plotted in Matlab, while the displacement results requires post-processing to eliminate the errors (i.e. laser jumps) due to disturbances in the laser-vibrometer. On the other hand, the results of the electric impedance experiment consist of magnitude and phase plots in frequency domain. No processing is needed in this case, the data are simply plotted in Matlab. However, a code based on a non-linear least-squares fitting routine is used to estimate the resistance and capacitance from the impedance data.

In contrary, a square signal input is used to actuate the robot during the free-swimming experiments. The motion of the robot is recorded on a camera, and the input voltage as well as the current consumption are recorded using a data acquisition system. First, the robot's motion is traced using a commercial motion trace software. This data needs to be filtered using a fifth order Butterworth filter, and then plotted in Maltab. A Matlab code is also used to extract the instantaneous and average velocities and accelerations, by using linear fitting methods. Second, the voltage and current consumption data are used to compute the power consumption. These results are then plotted in Matlab.

The bell kinematics design experiments are characterized in a similar way to free-swimming experiments. However, in this case the edge of the bell profile is detected and analyzed in Matlab. The outputs of this experiment are digitized bell profiles, curvature plots, and strain energy values.

2.2   Experimental setup for IPMC actuators

2.2.1   Electric Impedance Spectroscopy

Electrical impedance spectroscopy (EIS) is a measure of the impedance of a material across a range of frequencies. The impedance, $Z(j\omega)$, is a complex quantity where its magnitude represents the ratio of the amplitudes of the voltage (V) to the current (I) and the phase angle represents the phase difference between voltage and current. The complex electric impedance is defined in the following expression,

$$Z(\omega) = V(\omega)/I(\omega), \tag{2.1}$$

where ω is the frequency in radians per second (rad/s). However, in the case of a purely resistive circuit, the measured current is proportional to the applied voltage irrespective of the frequency. This is explained in the following expression,

$$V = IR, \tag{2.2}$$

where $R = Z(\omega)$ in this case since the impedance is purely resistive.

The impedances of an ideal capacitor and inductor are functions of frequency. The impedance of an ideal capacitor, C is $Z(\omega) = 1/j\omega C$, while the impedance of and inductor, L is given by the expression $Z(\omega) = j\omega L$. In reality many physical systems have complex electrical impedance that is not a single component as shown in the case of an ideal resistor, capacitor,or inductor. However, it is a combination of them and thus the circuit model of a system is not always trivial.

In order to understand the electrical behavior of the actuators at different frequencies, EIS measurements are performed. The hardware used for this purpose is AutoLab PGSTAT 12 Potentiostat and the FRA 4.9 software. The actuators are clamped in a cantilevered configuration by gold foil electrodes. The electrodes are in then connected to the AutoLab as shown in Figure 2.1. The applied voltage amplitide and frequency range for the measurement is 100 mV and 0.1 Hz-100 kHz respectively.
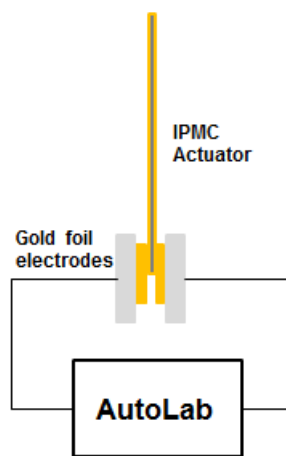
Figure 2.1: Schematic of the EIS measurments experimental setup.

2.2.2 Free Displacement

The bending behavior of the IPMC actuators, is tested using the experimental setup shown in Figure 2.2. A sinusoidal voltage waveform is used to excite the actuators. The actuators are clamped in a cantilevered configuration (Figure 2.2) by two gold electrodes. The resulting displacement is measured using a Polytec OFV-363 laser vibrometer and a Polytec OFV-3001 vibrometer controller at a point 20 mm from the clamped end.

The electrical measurements were done using a dSPACE data acquisition system (CP1104). A power amplifier is used to supply the voltage and current required for driving the actuators, while a non-inverting op-amp circuit is used to measure the current consumption as shown in Figure 2.3. Finally the free strain of the actuator is calculated according to the following expression,

$$\epsilon(t) = \frac{x(t)T}{l_f^2},\tag{2.3}$$

where $\epsilon(t)$ is the strain, $x(t)$ is the measured displacement, T is the thickness of the actuator, and l_f is the free length at which the laser was pointed and the displacement was measured.
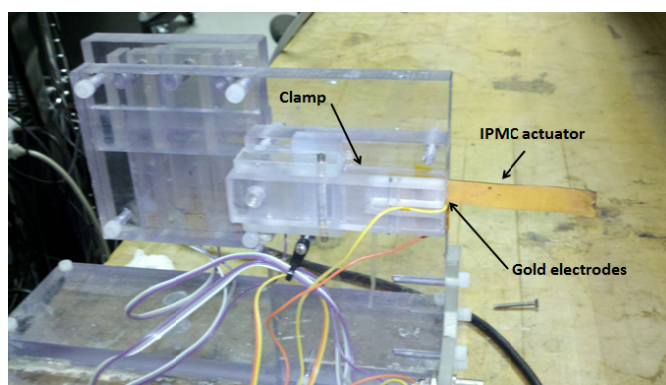
Figure 2.2: The experimental apparatus used to support the IPMC actuator for the EIS and Bending measurements.
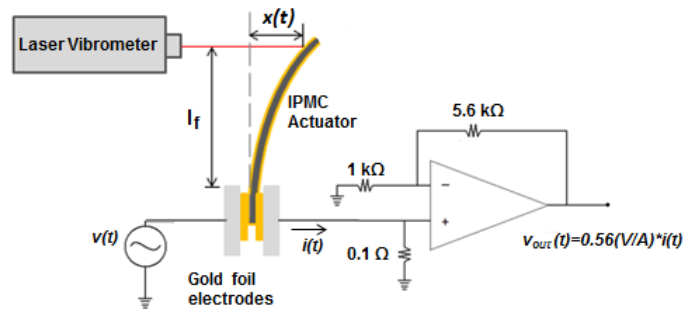
Figure 2.3: Schematic of the actuation characterization and current consumption measurement.

2.3 Robotic Jellyfish Experiments

2.3.1 Free-Swimming

The free swimming experiment is performed in order to test the swimming behavior of the robotic jellyfish. The experiments are carried out in two different water filled aquariums. First generations of the robots are tested in a 40 cm × 20 cm × 26 cm, while the last generation is tested in a 50 cm × 45 cm × 70 cm aquarium. Varying voltage waveforms are provided to the neutrally buoyant robot, and the resulting motion is recorded using a high-speed camera. The motion of the robot is tracked using a commercial motion trace software. The resulting data is then processed to measure the swimming speed of the robot as a function of the actuation parameters.

2.3.2 Bell Kinematics Experiments

Part of the biomimetic design process of the jellyfish robot, is to mimic the bell kinematics of the natural medusa. For this purpose the bell kinematics of the robot are designed based on a

systematic set of experiments. The experiments consist of varying the position of the IPMC actuator underneath the jellyfish bell. This will result in different deformation behaviors of the bell. A lab-built fixture (Figure 2.4) is used for this reason, the fixture will allow changing the position of the actuator in the x and y direction as well as the angle that the angle makes with the horizontal. A 0.5 Hz square wave input is applied to the actuator, the deformation is then recorded on a high speed camera. The videos are then processed in Maltab using a computer vision code that is written for the purpose of detecting the edge if the deformed bell. The results are then compared with the natural jellyfish bell deformation.
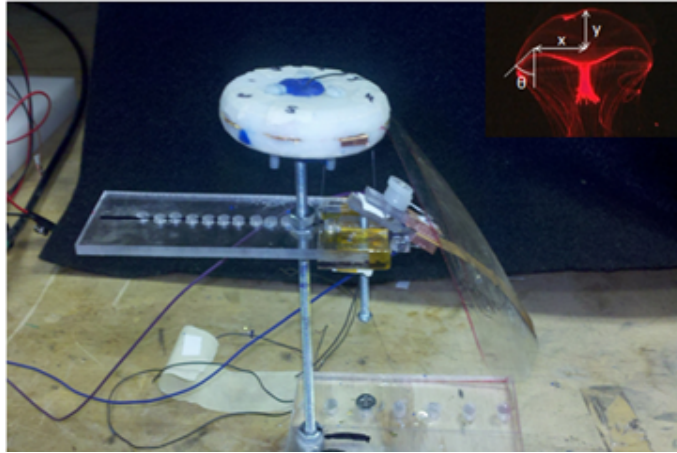
Figure 2.4: A picture showing the assembled experimental setup, at the top right is a picture of the actual Aequorea victoria which also shows what it is meant by x,y and θ.

2.4   Equipment Description

In the IPMC actuators set of experiments the ionic polymers were clamped at one end with two gold electrodes. These experiments are conducted in water, since they are water based. When not in use, the actuators are stored in deionized water. Figure 2.2 shows the

fixture used in both experiments, the fixture was acquired from previous researchers in the CIMSS lab. It is composed of two main lab apparatus,the clamp which is fabricated from plexiglass, and the circuit boards that contain the non-inverting op-amp circuit responsible of the current measurements.

In the EIS experiment only the clamp part of the fixture is used, while the full fixture is used for the free-displacement experiment. The impedance is measured by applying an AC potential, usually a sinusoidal wave, of known amplitude, $|V|$ and recording the resulting current flow. Therefore, the EIS measurements are carried out using AutoLab PGSTAT12 Potentiostat and the FRA 4.9 software. The frequency range of the applied potential (100 mV) is 0.1 Hz-100 kHz.

On the other hand, the displacement is measured using a Polytec OFV-363 laser vibrometer and a Polytec OFV-3001 vibrometer controller. The current consumed by the actuator is measured using a non-inverting op-amp circuit. The results of the voltage, current and the displacement are recorded using a dSPACE data acquisition system (CP1104). Note that the testings are done in water, thus the resulting displacement values are corrected by dividing them by 1.33. This number is equal the water refractive index, $n_{water} = 1.33$, and dividing by it will compensate for the change in the refractive index of teh laser signal across the air/water interface.

The robot swimming behavior is tested in commercial water filled aquariums(Figure 2.5). Different voltage waveforms are applied to the vehicle using a dSPACE data acquisition system. Subsequently, the voltage is amplified using an hp 6825 power amplifier, the resulting vertical motion is recorded using a Motion Scope PCI 2000S (RedLake Imaging) high speed camera. The videos are then processed with the Motion Trace software, that traces specific regions of the jellyfish while swimming. The current consumed by the robot is measured

using the same non-inverting op-amp amplifier used for the IPMC experiments. The voltage and current are recorded using the dSPACE data acquisition system. The actual power consumption is afterward computed using the recorded values of both the voltage and the current consumption. Note that all data are processed and plotted in Matlab.

Finally,the bell kinematics design experiments are achieved using a lab-built fixture. It consists of the following parts: a central hub, an IPMC actuator, a slice of a symmetric bell (one eighth of the full bell), and a stage that serves to change the location (x and y) and angle of the actuator which is located underneath the bell. Figure 2.4 shows a photographic picture of the apparatus. The characterization process is similar to the free-swimming experiments, however, a computer vision Matlab code is used to detect the motion of the bell instead of the Motion Trace software.

Figure 2.5: A picture of the experimental setup used to test the swimming behavior of the jellyfish.

Chapter 3

Ionic polymer metal composites fabrication and characterization

The actuators used to deform the bell of the jellyfish robot, are ionic polymer metal composites (IPMC). As mentioned in Chapter 1, IPMCs are chosen because of their ability to bend at high strain percentage (5%) when a low potential (2V-5V) is applied [27].

IPMC actuators are fabricated using the Direct Assembly Process (DAP) that was developed by Akle et al [21]. The DAP method has been extensively used and optimized for fabricating dry IPMCs , however, the fabrication of water-based IPMC using DAP is recent and requires optimization. In this chapter, the fabrication process based on the DAP method is explained and described. Moreover, optimization experiments that focus on the effects of the electrodes thickness, the number of platinum layers deposited on the electrodes, and the chemical composition of the electrodes on the performance of the actuators are discussed. Finally, a summary of the experimental bending and impedance measurements results is presented.

3.1   IPMC Actuators Fabrication Method

An ionic polymer metal composite consists of a bare semi-permeable membrane, sandwiched between two conductive, high surface area electrodes. In the DAP method (Figure 3.2), the membrane is soaked in a sodium hydroxyde (NaOH) solution, which will lead to an ion exchange from the proton counterion(H^+) form to one of the alkali metal form (Na^+ in this case). This is done in order to prevent charring of the membrane during the drying step. Afterwards, the membrane is left to dry in an oven at a temperature of 150 ^{o}C, and under vacuum for around 12 hours [21, 27, 28].

Meanwhile, the electrode solution which is an ion conducting polymer/metal solution is prepared. The mixture consists of a 10% Nafion solution that was purchased from the FuelCellStore, ruthenium dioxide (RuO_2) powder, Single Walled Carbon Nanotubes (SWNT), gold nanoparticles, and a particle dispersion mixture. The dispersion mixture is made of the following: 50 wt% Deionized water, 25 wt% Isopropyl Alcohol, and 25 wt% Ethanol. Note that the composition of the electrode material as well as the dispersion mixture are acquired from Akle et al [21]. However, the difference in this case is adding gold nanoparticles in some cases. SWNT is meant to provide large surface area (up to 1000 m^2/g),but it is relatively less conductive when compared to gold nanoparticles, thus we believe that adding the gold nanoparticles will improve the performance of the actuators by increasing the internal electrical conductivity. The full solution is mixed, stirred and sonicated.

Once the membrane is dried, the solution is sprayed directly onto each surface.The membrane lays on a vacuum table underneath an Infra Red lamp. The IR heating of the sample will help dry the membrane faster by evaporating the water and the alcohol solvents. After the spraying process is complete the sprayed membrane is dried at 130°C under vacuum for one hour which will insure the compete evaporation of all volatile components of the electrode
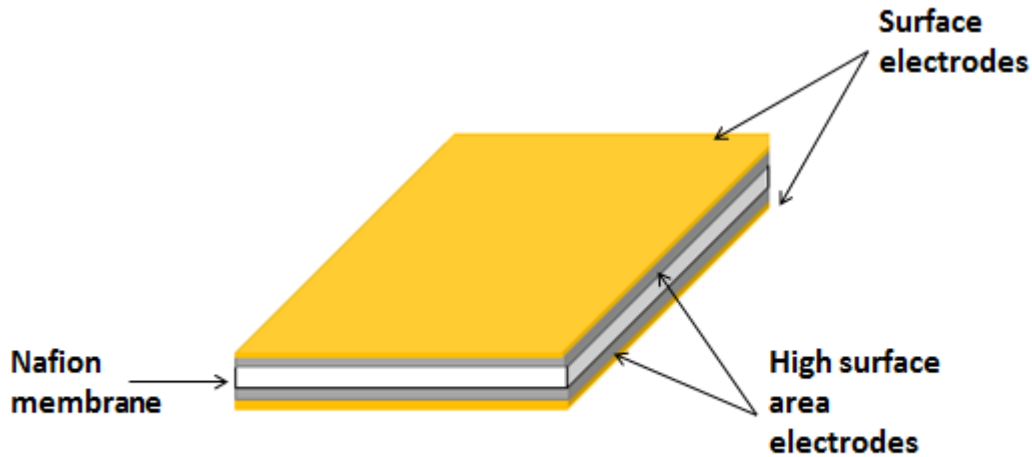
Figure 3.1: Schematic of the IPMC showing the Nafion membrane sandwiched by the high surface area electrodes,in turn sandwiched by the Platinum/Gold surface electrode.

material.

The next step after drying the sample is to melt-press it at a temperature of 210^oC and a pressure of approximately 206.84 Mpa. The sample is pressed for a total of four minutes (two minutes for each side), in order to insure uniformity in the sample. The membrane is now sandwiched between two high surface area electrodes. As mentioned above the electrodes are composed of RuO_2, SWNT and gold nanoparticles in a matrix of Nafion polymer. Figure 3.1 shows a schematic describing the structure of the IPMC.

Oguro et al. [29], proved that an increase in strain per unit voltage is correlated with an increase in the number of platinum layers added to the polymer. This is due to the increase in the conductivity of the high surface area electrodes. For this purpose, platinum layers are added to the electrodes using the impregnation-reduction method [29] which consists of two main steps. The first is to saturate the full membrane with $Pt(NH_3)_4{}^{2+}$ by soaking the polymer in a tetraammineplatinum chloride solution. The next step is to soak the membrane

in a sodium borohydride solution ($NaBH_4$), this will reduce the metal salt on the surface of the membrane. The reduction process is done in a cold environment, a bath of ice is used in our case, to slow the ion reduction process and thus insure more deposition on the surface of the electrodes. Sodium borohydride is gradually added, its concentration starts at 0.2 wt% and increases by 0.2 wt% every 30 minutes, this process is repeated five times.

The last step in the process is to increase the surface conductivity by deposit a thin layer of gold on the electrodes. An electroplating gold solution is used for this purpose, the IPMC samples are plated until the surface resistance is reduced below 1Ω. A last step might follow the metal deposition process, and consists of exchanging the mobile cation in the polymer by any other convenient ion (Na^+ in this case) by soaking the polymer in the corresponding salt solution (NaCl in this case). This process is complete at this stage and is done in aqueous solutions with the IPMC membrane in a water-saturated state.

3.2   Study on Improving IPMC Peak to Peak Bending Strain

The Direct Assembly Process (DAP) of ionic polymer metal composites is used in this thesis. However, as mentioned in the previous section, the DAP method has been optimized for fabricating dry IPMCs. Therefore the water based IPMC requires additional optimization. Akle et al. provided an optimization study for the dry IPMC, similar techniques are used in this case. In addition, the DAP provides control on different variables in the polymer fabrication process. In this section, some of these variables are inspected and optimized. The variables studied in this case are the electrode thickness, the number of platinum layers and the electrodes chemical composition.
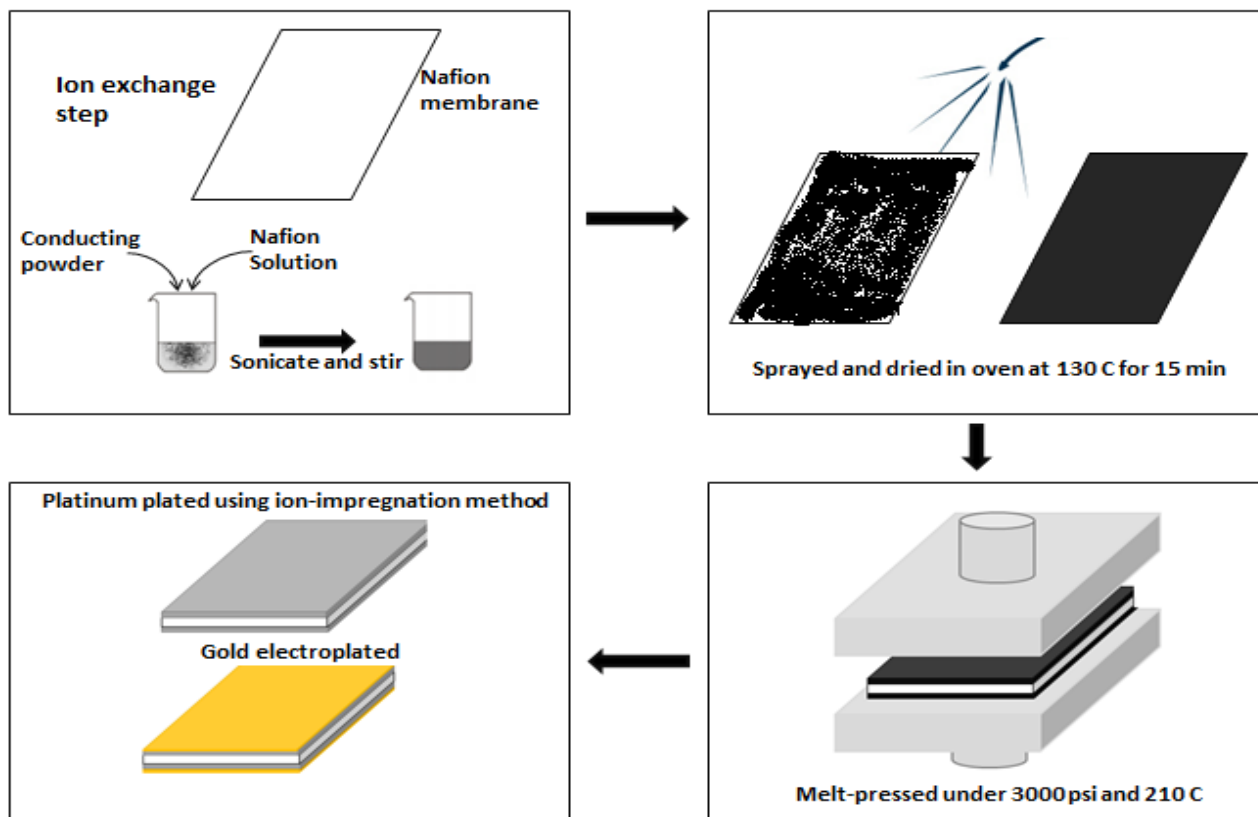
Figure 3.2: Schematic showing the four step needed to fabricate a water-based IPMC using DAP method.

In the first experiment, the thickness of the electrode is varied, and subsequently the tip displacement is measured. The number of platinum layers is varied in the second experiment. In the last set of experiments the chemical composition of the electrodes is varied. Finally, the combination of the three different parameters at different level each is also tested, in order to account for any coupling effect that might happen among the three variables. For this purpose, the Taguchi method [30] is used in order to design the experiments.

3.2.1 Effect of Electrode Thickness and Applied Pressure

In this experiment the thickness of the electrode is increased while maintaining the same chemical composition of the electrodes. In the first set of experiments two samples with $30\mu m$ and $65\mu m$ thicknesses are fabricated, the chemical composition of the electrodes consists of 35% RuO_2 and 10%SWNT. The samples are melt-pressed for four minutes at 3,000 psi and 210^oC. The strain response of these samples increases with the thickness of the electrodes. Figure 3.3 shows the strain results of both samples. It is shown that the peak to peak strain value of the $30\mu m$ sample (0.048 %) is lower than that of the $65\mu m$ (0.1 %).
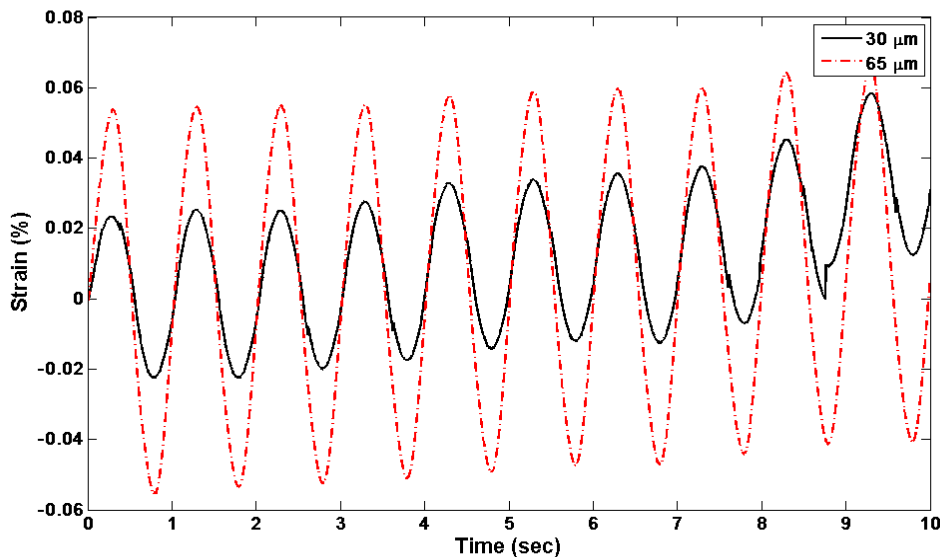
Figure 3.3: Strain response of two samples with different electrode thickness when a 2V, 1 Hz sinusoidal wave is applied.

This result shows that the higher the thickness the higher the peak to peak strain. This is due to the fact that the amount of particles and the interface area are proportional to the thickness of the electrode. Akle et al. [21] showed that the strain response and the electrical capacitance of the IPMC are correlated in a linear fashion. Akle explains this process by

the fact that the low-frequency capacitance of an IPMC is related to the charge transport and accumulation at the blocking electrode which will lead to a mechanical deformation. Therefore, adding more particles by increasing the thickness of the electrode, will increase the polymer capacitance and thus result in higher peak to peak strain response. Note that strain results are found to be proportional to the thickness of the electrode which confirms with the results published by Akle previously [24, 20].

The applied pressure during the melt-press step is also studied. As was shown in the previous experiment, the higher the thickness, the higher the peak to peak strain response. However, the drawback from increasing the thickness of the electrode is increasing the mechanical stiffness of the IPMC. One way of reducing the stiffness while keeping the same electrode thickness is to decrease the overall thickness of the IPMC. This is due to the fact that stiffness is proportional to the cube of the thickness of a cantilevered beam and shown in Equation 3.1,

$$k = \frac{Ebt^3}{12L^3},$$
(3.1)

where k is the beam stiffness, E is the modulus of elasticity, b is the width of the beam, t is the thickness of the beam, and L is the length of the beam.

Two samples are also fabricated for this experiment. The samples have the same chemical composition (35 % RuO_2 and 10 % SWNT), the same number of platinum layers (one layer), and the same size. The only difference is that one of the samples is pressed at 3,000 psi and the other at 5,000 psi. Figure 3.4 shows the strain response results due to a 2V, 1 Hz sinusoidal wave input. The sample that was pressed at 5,000 psi exhibits higher peak to peak strain (0.23 %) as opposed to (0.1 %) for the other sample. As a conclusion the strain response of the IPMC is improved by increasing the thickness of the electrodes and decreasing the overall stiffness by melt-pressing at higher temperature.
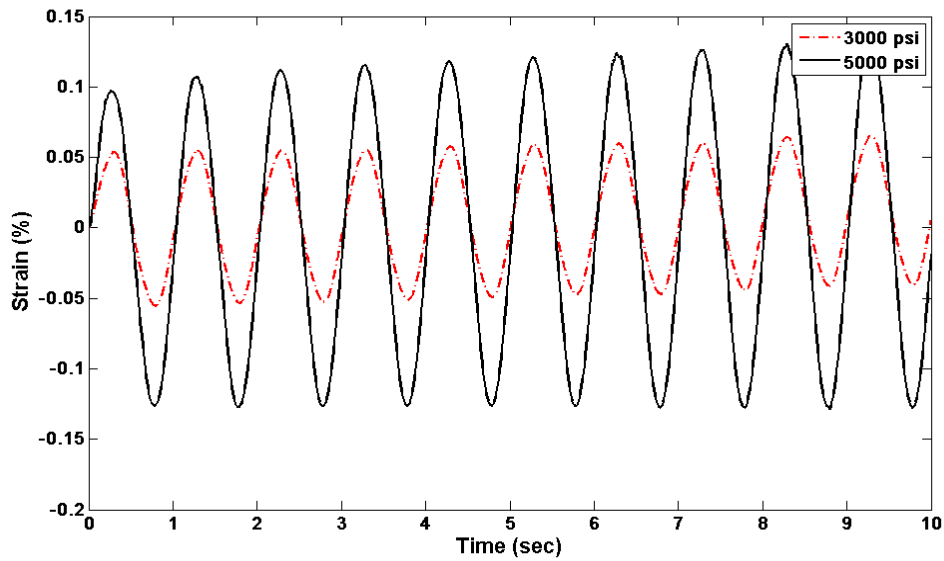
Figure 3.4: Strain response of two samples melt-pressed at two different pressures when a 2V, 1 Hz sinusoidal wave is applied.

3.2.2   Effect of Number of Platinum Layers

The impregnation-reduction method is used to deposit platinum layers at the surface of the IPMC electrodes. The method is explained in details in section 3.1. Nemat-Nasser et al [31] demonstrated that the depth and the uniformity of the electrodes affects the performance of the IPMC. Therefore, controlling the depth of the penetration inside the electrodes, by varying the concentration of the reducing agent, will improve the performance of the polymer. Another parameter to optimize for the impregnation-reduction method, which in turn will lead to optimizing the IPMC, is the number of platinum layers. Oguro et al [29], proved that increasing the number of platinum layers will increase the strain per unit voltage. However, this improvement is limited by the increase in the mechanical stiffness of the electrode that reduces the deflection.

Three samples are fabricated using DAP method. The samples are composed of (25% RuO_2

and 10% SWNT), the thickness of the electrodes is $65\mu m$, and they are melt-pressed at 5000 psi and 210^oC for 4 minutes. One platinum layer is added for the first sample, two for the second, and three for the last. Figure 3.5 shows the strain response due to a 2 V, 1 Hz sinusoidal wave voltage input. The plot shows a significant increase in peak-to-peak strain response from the one layer sample (0.042%) to the two layer sample (0.0995%). A smaller increase is also shown from the two layers to the three layers (0.123%) samples. This is explained by the increase in mechanical stiffness that opposes the increase in deflection due to the increase in platinum layers.
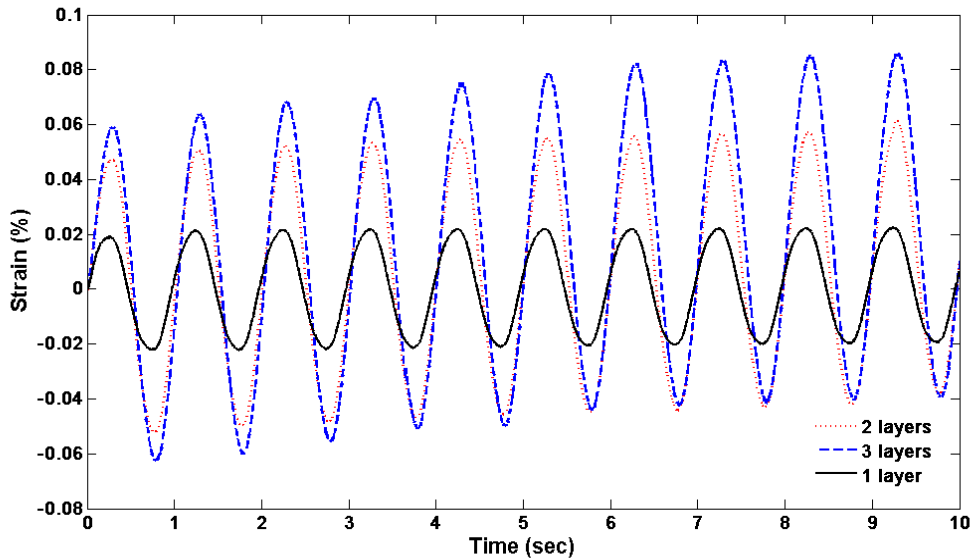
Figure 3.5: A plot showing the strain response of the three different samples with different platinum layers.

3.2.3 Electrodes Chemical Composition

Direct assembly process for fabricating the ionic polymer metal composites enables the ability to introduce different chemicals to the electrode structure. Traditionally, platinum and gold

are used as electrode materials [32]. There are also some attempts in literature to use copper, silver and nickel [28]. However, ionic polymer transducer electrodes developed by Akle et al [21] are composed from ruthenium dioxide (Ruo_2) and single wall carbon nanotubes (SWNTs).

Ruthenium dioxide was first used by Leo's research group for developing actuators. RuO_2 is a less expensive material compared to other noble metals. Moreover, RuO_2 is interesting in our case because it has a typical specific capacitance of $80\mu F/cm^2$. This will enable the fabrication of electrodes with higher capacitance and consequently higher bending deformation. On the other hand, SWNTs have large effective surface area up to $1000m^2/g$. Moreover, carbon nanotube actuators generate large forces and small strains, and they bend towards the anode (+), which is the same direction as the IPMC. These reasons make SWNTs good candidates to be used as electrode materials, and this has been proven by Akle et al in his paper [33].

However, the electrical conductivity of the SWNTs is relatively low and is highly dependent on the purity of the carbon nanotubes. Therefore, in our case gold nanoparticles are added to the chemical composition of the electrodes. Gold nanoparticles are highly conductive (454500 S/cm), but their major disadvantage is the low surface area (0.4 to 0.75 m^2/g). The addition of gold particles is meant to increase the conductivity of the electrodes and thus compensate for the relatively low conductivity of the SWNTs. The carbon nanotubes in turns compensate for the low surface area of the gold nanoparticles.

Four samples are fabricated for this experiment. The thickness of the electrodes of the four samples is the same ($65\mu m$), with the same dimensions (2×0.5 cm). In addition, all samples are melt-pressed at 34.47 Mpa and 210^oC for 4 minutes. Table 3.1 summarizes the chemical composition of each sample. The first sample is only composed from RuO_2 (50 vol.%), this

is done in order to test the effect of SWNT and Gold nanoparticles on the deflection of the actuators. For the second sample SWNT is added to ruthenium dioxide, in the third gold nanoparticles are added to ruthenium dioxide and finally the fourth is composed from the three materials tested in this experiment.

Table 3.1: The chemical composition of the four samples.

Sample	RuO_2	SWNT	Gold nanoparticles
1	50 vol.%	-	-
2	35 vol.%	15 vol.%	-
3	35 vol.%	-	15 vol.%
4	25 vol.%	15 vol.%	10 vol.%

Figure 3.6 shows the strain response of the sample actuators due to a 2V, 1 Hz sinusoidal wave voltage input. The highest peak-to-peak strain value achieved is 0.2622% and it corresponds to sample 4 as defined in Table 3.1. The addition of SWNT to the electrode chemical composition does improve the strain response from 0.1750% (RuO_2 only) to 0.2349%. Similar increase is shown also when Gold nanoparticles are added where the maximum peak-to-peak strain value achieved is 0.21%.

3.3 Jellyfish Robot Actuators Characterization Results

In this section, the actuators used to propel the jellyfish robot are characterized in order to keep track of each actuator's performance and test its effect of the overall behavior of the robot. DAP manufacturing process is used to fabricate the actuators. Further explanation is given in Section 3.1. Each electrode layer is $65\mu m$ thick and consists of a mixture of 25 vol.% ruthenium dioxide (RuO_2), 15 vol.% single wall carbon nanotubes (SWNT), 10 vol.% gold nanoparticles and 50 vol.% Liquid Nafion. The original sheet size is (10 x 7 cm), the
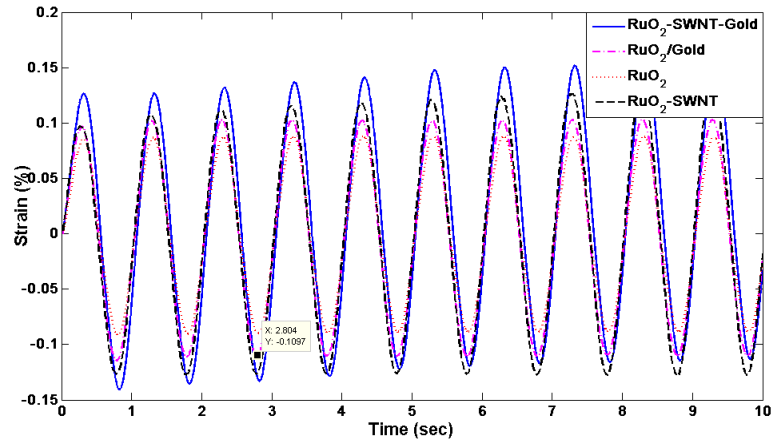
Figure 3.6: A plot showing the strain response of the four different samples with different chemical composition.

sheet is melt-pressed at $210^{o}C$ and a pressure of 30,000 psi. Three layers of platinum are then applied to the electrode material using ion-impregnation method discussed in Section 3.2. Finally, the plated material is divided into 10 equal-sized actuators. The shape of each actuator is rectangular and the dimensions are (6.5 x 1 cm) with an approximate thickness of $22\mu m$. The electrical impedance and bending performance (in air and water) of each IPMC actuator are experimentally measured. As mentioned in sChapter 2, Akle and Leo[REF] demonstrated that IPMCs exhibit a linear relationship between the strain and the electrical capacitance. Therefore, EIS measurements and free bending experiments are performed in order to understand the electrical behavior of the actuators using the experimental setup discussed in Chapter 2.

Generally, the actuators exhibit a flat magnitude at frequencies above 1 Hz. Figure 3.7 shows the through thickness magnitude and phase angle results of the electrical impedance versus frequency for each actuator. On the other hand, the phase angle data show a decreasing negative phase angle below 1 Hz and a phase of approximately zero at higher frequencies. Based on this information, we assume that the actuators exhibit a capacitive behavior at
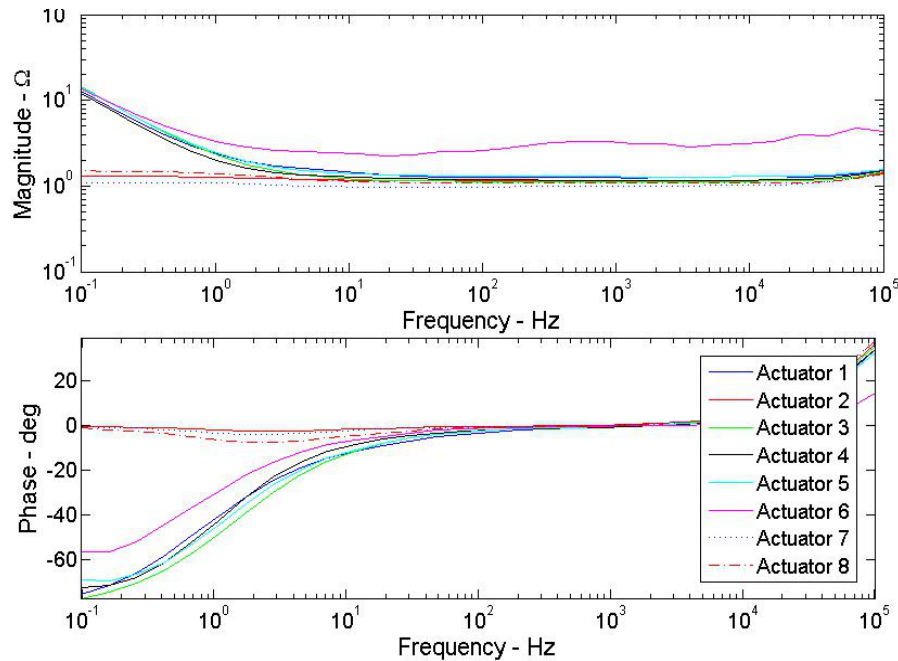
Figure 3.7: Magnitude (top) and phase angle (bottom) of the electrical impedance magnitude verses frequency for each of the eight IPMC actuators.

low frequencies ($< 1Hz$). In contrast, the actuators act as resistors at higher frequencies.

The bending behavior of the IPMC actuators is also tested. The strain response varies for different actuators. Actuator 1, shows the highest peak-to-peak strain of 0.747% when actuated at 1 Hz, 0.839% when actuated at 0.5 Hz and 0.88% when actuated at 0.1 Hz (Table 3.2). In contrast, actuators 6, 7 and 8 exhibit peak-to-peak strains of only 0.37% at 0.5 Hz. On the other hand, the actuators are also tested in water since the main application is in water. The actuators exhibit less strain percent for the same applied signal (2V and 0.5 Hz). Figure 3.8 shows the measured strain of each of the eight actuator in water. Table 3.2 summarizes the peak-to-peak strain results and capacitance values for the actuator. The reason this study is conducted is to show how well the capacitance is correlated with the strain. The capacitance values are given for actuator 1 and 3 through 6. Most actuators act as capacitors at frequencies less than 1 Hz. However actuators 2, 7 and 8 behave more

Table 3.2: Measured electrical capacitance values and peak-to-peak strain results.

		Peak-to-Peak strain (%) results					
		0.1 Hz		0.5 Hz		1.0 Hz	
Actuator	Capacitance (F)	Air	Water	Air	Water	Air	Water
1	0.115	0.880	0.742	0.839	0.671	0.747	0.565
2	-	0.522	0.556	0.479	0.336	0.324	0.279
3	0.100	0.598	0.640	0.463	0.386	0.371	0.327
4	0.126	0.850	0.646	0.742	0.550	0.538	0.460
5	0.104	0.607	0.455	0.504	0.420	0.425	0.364
6	0.117	0.394	0.315	0.362	0.289	0.327	0.261
7	-	0.351	0.339	0.448	0.308	0.340	0.241
8	-	0.356	0.343	0.476	0.390	0.398	0.287

resistively across the frequency range tested, as shown by the flat magnitude of impedance and phase angles at frequencies less than 10 Hz. On the other hand, each actuator exhibits higher strain at the lowest excitation frequency (0.1 Hz) in water and in air. The peak-to-peak strain reduces gradually with increasing the frequency.

3.4 Chapter Summary and Conclusions

In this chapter the fabrication, optimization, and characterization of water-based IPMC actuators using the DAP process were presented and thoroughly explained. The electrode optimization results demonstrated that increasing the thickness of the electrode would result in an increase in the strain percent response of the actuator. This result was consistent with the results obtained by Akle et al. which demonstrate a linear relationship between the thickness of the electrode and the strain percent response. The optimization results also proved that an increase in the strain response occurred as a result to an increase in the pressure applied during the melt-pressing step.

The electrode was also optimized on the chemical level. The results show that adding three
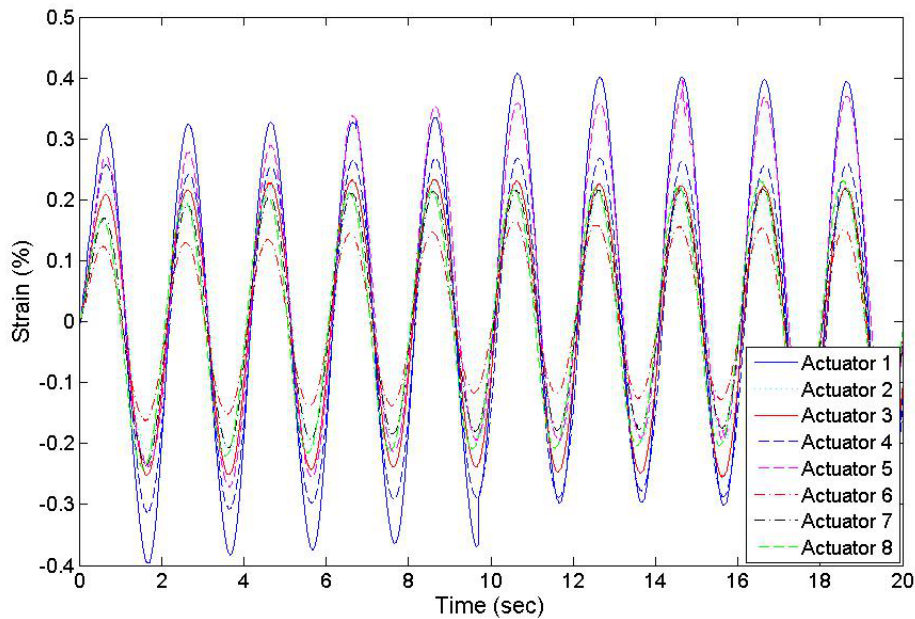
Figure 3.8: Strain response versus time of the actuators in water for an applied 2V at 0.5 Hz.

layers of platinum increased the strain response of the actuator. On the other hand, the addition of gold nanoparticles proved to improve the strain response of the actuator as well as the addition of SWNT. The resulting optimized chemical composition of the electrode is as follows: 25 vol.% ruthenium dioxide (RuO_2), 15 vol.% single wall carbon nanotubes (SWNT), 10 vol.% gold nanoparticles and 50 vol.% Liquid Nafion.

In order to check the consistency of the actuators used for the jellyfish robot, eight different IPMC actuators were fabricated and characterized in air and in water. The results show that highest peak to peak percent strain achieved was 0.88 % in air at 0.1 Hz frequency, 0.839% at 0.5 Hz, and 0.747 % at 1 Hz. Note that in the introduction it was mentioned that the IPMC actuators can achieve up to 5% strain. The reason we are not achieving this number is due number f reasons. First, the actuation frequencies we are using are relatively high and with a slow response rate it is hard to achieve high strain values. Second, the

water-based actuators we are manufacturing using the DAP process for the first time and need more optimization.

Chapter 4

Analysis and Design of a Biomimetic Bell

The jellyfish bell kinematics play an important role in determining the swimming style of the medusa. As explained in Chapter 1, jellyfish species are classified under two main types, "Oblates" and "Prolates". Oblate species are more efficient compared to the prolates since they propel their body using the rowing propulsion technique. Rowing propulsion technique is based on generating both stopping and starting vortices during swimming. These two different types of vortices are the result of the non-uniform bell contraction of oblate species [12].

Bell kinematics determine the propulsion technique and thus affect the swimming speed and efficiency of the jellyfish [14]. For this purpose, in the first section of this chapter, a comparative bell kinematics analysis is conducted between the natural *Aurelia aurita* and the *Aequorea victoria* medusae. In the second section, a discussion of a biomimetic bell kinematics design is presented. This section focuses on the design and characterization of a

bio-inspired bell, that mimics the morphology and kinematics of the natural jellyfish.

4.1   Comparative Bell Kinematics and Geometry Study: *Aequorea victoria* vs. *Aurelia Aurita*

In this section a comparative study on the bell kinematics and morphology of the *Aequorea victoria* and the *Aurelia aurita* is presented. First, the methods of quantifying the bell deformation are described. Secondly, a comparative study of both bell morphologies and deformations is presented. Finally, since energy is of an important interest in our case, the strain energy stored in the bell of both medusae during the contraction phase is analyzed and compared.

4.1.1   Methods of Quantifying Bell Deformation

Two different methods are developed to analyze medusae bell profiles during the relaxation and contraction phases. The first method represents a first order study that is usually used by biologists to measure the relative deformation of the bell at a small number of points. The second is a more sophisticated method that consists of computing the radius of curvature at different points of the bell.

Percent Bell Contraction

This method consists of measuring the bell deformation at different locations along the length of the bell profile. The next step is to compute the percent bell contraction relative to the

bell shape during the relaxation phase. This method represent a rough method to study bell shape and contraction behavior, and help understanding the bell deformation distribution along the length of the bell. Costello et al [14] adapted this methods in many of his papers and studies on jellyfish bell morphology and swimming properties. This method also helps comparing the kinematics of the bell of different species.

Radius of Curvature

The second method used in quantifying the deformation of the jellyfish bell profile, is the radius of curvature. This method is more accurate compared to the percent bell contraction method since it is related to the geometry of the bell and results in higher resolution quantitative comparison between two different medusae. Obtaining the radius of curvature at different points along the bell profile, allows us to quantify the different profiles achieved by the natural species or by the robot. Moreover, the strain energy stored in the bell during the contraction phase can also be computed using the curvature ρ defined as the inverse of the radius of curvature. Computing the strain of energy help to quantify any potential differences in the actuation requirements of the robot bell. The radius of curvature is defined as the radius of the approximating circle, and is defined by the following expression,

$$R = \frac{[1 + (\frac{dy}{dx})^2]^{3/2}}{|\frac{d^2y}{dx^2}|},$$
(4.1)

where R is the radius of curvature of a curve defined by the relationship $y = f(x)$.

In our case, the equation of the bell profile is not defined and an approximation method is needed in order to approximate the radius of curvature. There are three different methods that are usually used for this purpose, but the most accurate is the "3 Points" method since

it is based on finding the equation of the circle passing through three consecutive points [34]. This method computes the exact value of the radius of curvature the circle based on the obtained circle equation. The radius of a circle passing through three different points is defined as the distance from any of these points to the center of the circle. Equation 4.2 is used to compute the radius of curvature assuming that the coordinates of the center are known,

$$R = \sqrt{(x_i - x_c)^2 + (y_i - y_c)^2}, \tag{4.2}$$

where x_i and y_i are the coordinates of any of the three points that lay at the circumference of the circle of center (x_c, y_c). Given three points on the circumference, the expressions for the center of the circle are,

$$x_c = \frac{m_1 m_2 (y_1 - y_3) + m_2 (x_1 + x_2) - m_1 (x_2 + x_3)}{2(m_2 - m_1)}, \tag{4.3}$$

$$y_c = -\frac{1}{m_1}(x_c - \frac{x_1 + x_2}{2}) + \frac{y_1 + y_2}{2}, \tag{4.4}$$

where m_1 and m_2 are the slopes of the lines L_1 joining points 1 and 2, and L_2 joining points 2 and 3, respectively (Figure 4.1). The slopes are defined as follows,

$$m_1 = \frac{y_2 - y_1}{x_2 - x_1}, \tag{4.5}$$

$$m_2 = \frac{y_3 - y_2}{x_3 - x_2}. \tag{4.6}$$

Further explanations on the derivations of the equations mentioned in this section can be found in mathematics books and in literature [34].
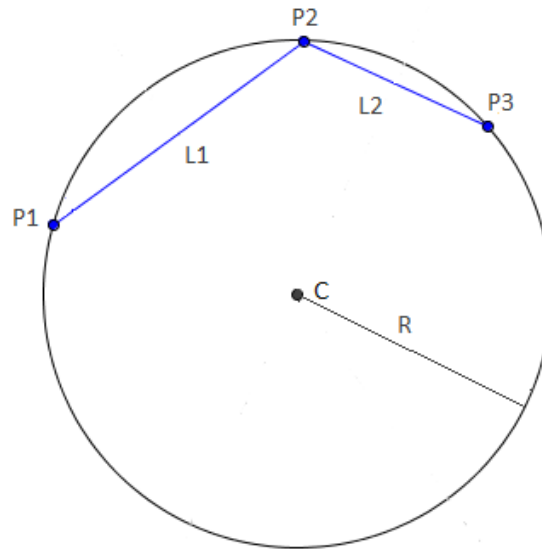
Figure 4.1: Radius of curvature calculation using a geometrical approach the "3 Points" method

4.1.2   Video Processing and Edge Detection

Videos for different swimming jellyfish species were provided by Jack Costello, Providence College and Sean Collin, Roger Williams University. The videos are converted into images using either VirtuaDubMod 1.5.10.3 software or a computer vision code that is written in Maltab. Points along the bell exumbrella (the exterior side of the bell) are extracted using edge detection techniques provided by Maltab as shown in Figure 4.2. For each frame, the coordinates the the bell summit are set to (0,0) to be used as a reference point. This is done by subtracting the original coordinates of the apex point from all the points along the profile of the bell. This process is done at the full contraction and relaxation positions. The data is then normalized by the length of the profile for consistency.

The radius of curvature method calculates the radius of curvature using a discrete number
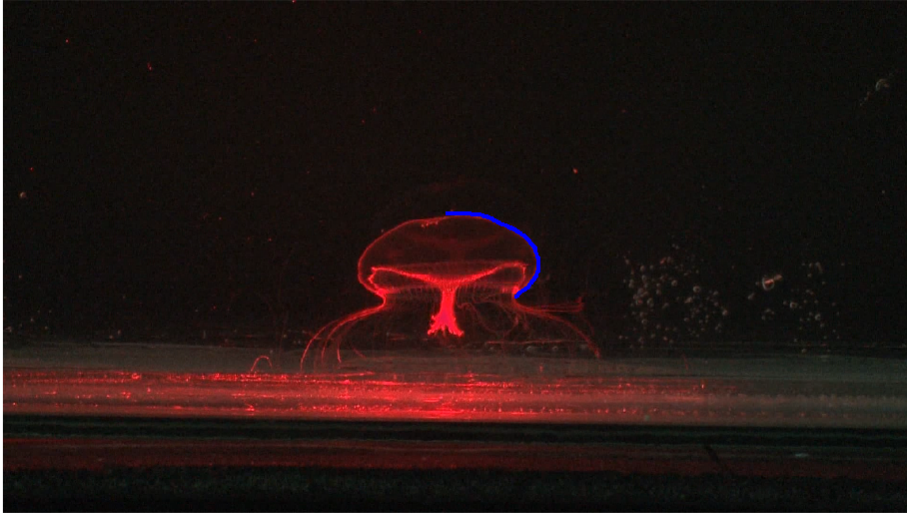
Figure 4.2: Image of *Aequorea victoria* specimen where its bell is fully contracted, the automatically detected points are shown as blue dots.

of points these points are detected using computer vision techniques and in reality they represent the pixels of the analyzed frame. This will cause errors and inaccuracy in the values of the computed radius of curvature values since this method is very sensitive to the coordinates of the points used in the process. Therefore, a curve fit is done through the points in order to obtain the coordinates of any point on the profile of the bell. Sixth and seventh order polynomials are used for the curve fitting. The coordinates are expressed in terms of l which represents the position along the profile length, and have the form as shown in the following,

$$x = f(l) = a_o + a_1 l + a_2 l^2 + ... + a_n l^n, \tag{4.7}$$

$$y = f(l) = b_o + b_1 l + b_2 l^2 + ... + b_n l^n, \tag{4.8}$$

where x and y are the coordinates of any point along the profile of the bell, and n in the order of the polynomial used to curve fit the original data.

Once the points from the curve fitted data are obtained, the formulas discussed in Subsection 4.1.1 are used to compute the radius of curvature. As previously mentioned the 3-points method computes the radius of curvature passing through three consecutive points. Therefore, multiple points of interest on the profile are chosen as shown in Figure (4.3) where the points of interest are in blue. These equally spaced locations are ten points apart. This is done in order to reduce the overall sensitivity of the calculations. The curvature is then obtained according to Equation 4.9,

$$\rho = \frac{1}{R}. \tag{4.9}$$

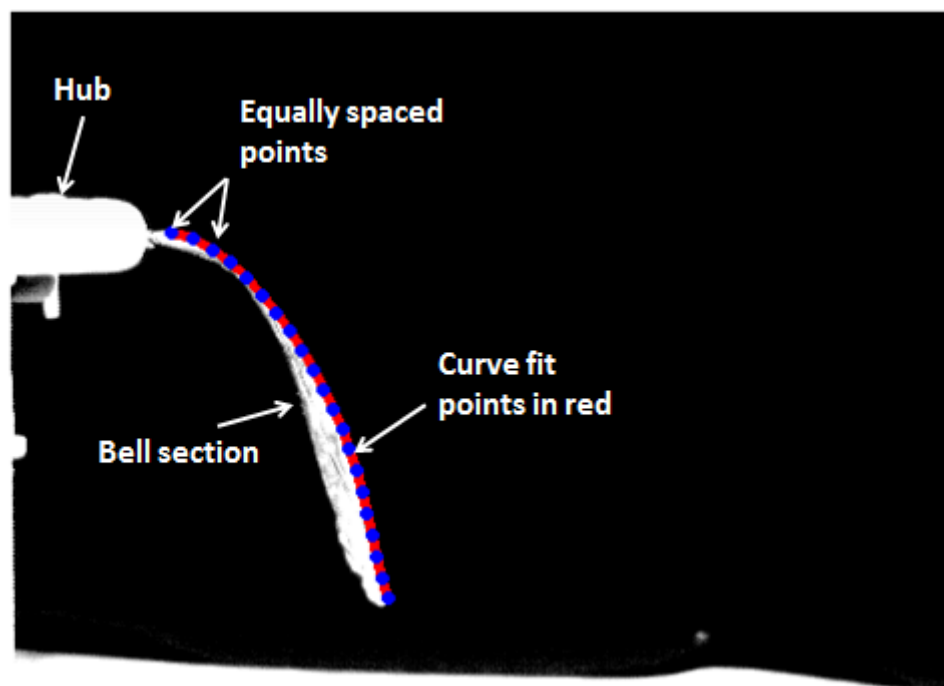Figure 4.3: Image of the digitized bell profile showing the curve fitted points in red and the points of interest used to compute the radius of curvature in blue.

4.1.3   Bell Morphology and Deformation Comparison

The morphology and kinematics of the jellyfish bell play an important role in the swimming behavior and propulsion properties of the natural medusa. Therefore, this section presents an analytical and quantitative study of the bell geometry of two oblate species, the *Aequorea victoria* and the *Aurelia aurita*. These species are chosen since they both are oblates, and since information about these animals is available in the literature. The purpose of this study is to understand both medusae structures and swimming behaviors in order to chose the species that best fit the properties of the IPMC actuator that are used in this project.

Bell Geometry

Figure 4.4 shows the bell shapes of both medusae. These plots represent the digitized bell profiles at both the full relaxation and contraction states of the bell for each species. In the relaxation state, the *Aurelia aurita's* bell, represented by the solid black line, roughly takes an elliptical shape, where it is relatively flat at the top but abruptly curves toward the margin. On the other hand, the *Aequorea victoria*, represented by the dash-dotted line, has a more spherical shape, where the curvature does not exhibit any abrupt changes along the length of the profile.

This is also shown in Figure 4.5, which shows two different curves representing the bell curvature at the relaxed state for both medusae. The curvature of the *Aurelia aurita* bell, represented by the solid black line, is low and constant at the first half of the bell (ρ 1 u^{-1}). However, it changes abruptly in the second half where it starts to increase and reaches its maximum around the bell margin. In contrast, the *Aequorea victoria* represented with the dash-dotted line, exhibits a more or less constant curvature where it varies between (2 and

3 u^{-1}) with also the highest located at the bell margin. Note here that (u) stands for unity since all dimensions in the plots are normalized by the length of the bell profile.

Understanding this difference in bell geometry is important since it will help in choosing the medusa that best fits the requirements of our design. In addition, it is believed that the position at which the IPMC actuators are implemented affect their performance. Therefore, one shape of the jellyfish bell might be more convenient to fit this property of the actuators, and thus improve the propulsion performance of the robot.
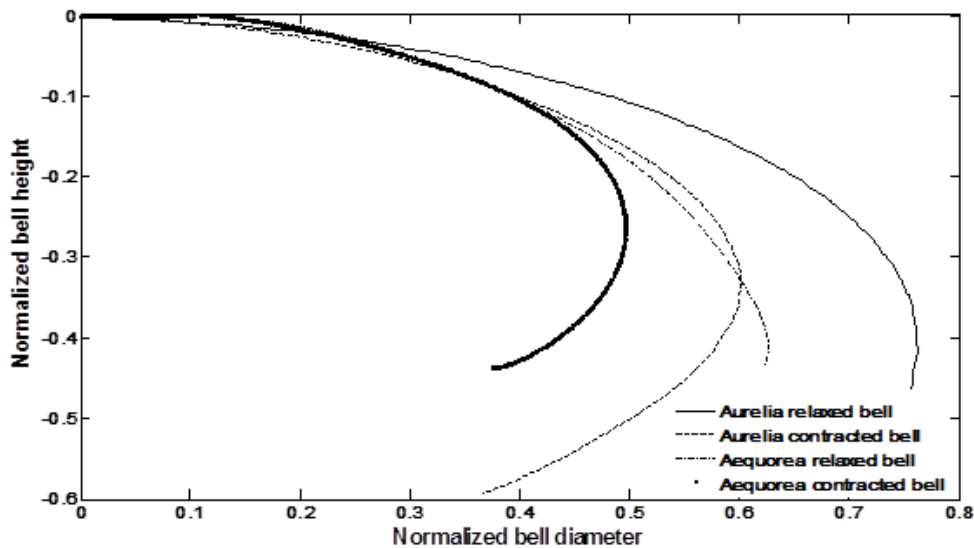
Figure 4.4: A plot showing the relaxed bell profile as well as the contracted profile for both the *Aurelia aurita* and the *Aequorea victoria*.

Bell Deformation Behavior and Fineness Ratio

In addition to the bell geometry, the bell deformation behavior is also an important criteria to study. As mentioned before, the propulsion properties of the medusae highly depend on the kinematics of the bell. Figure 4.4, shows the fully contracted bell of the *Aurelia*
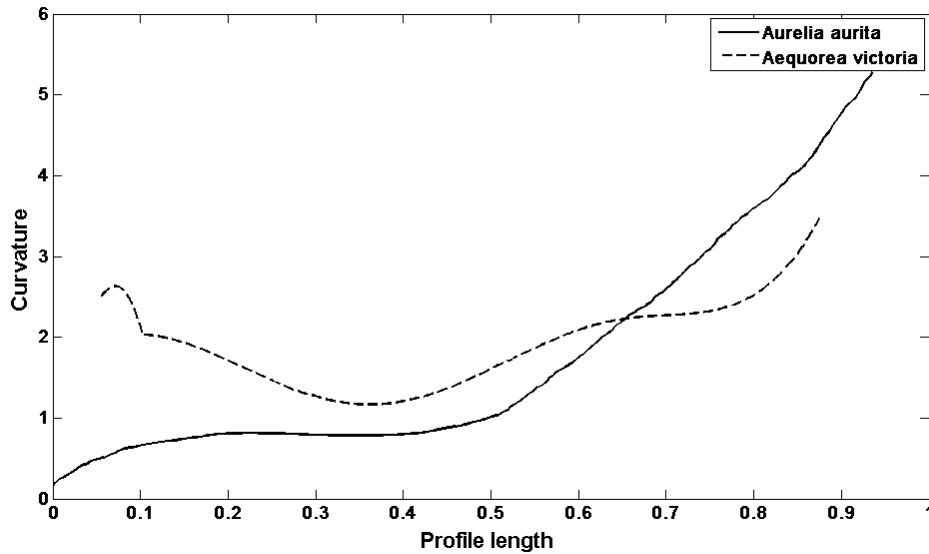
Figure 4.5: A plot showing the curvature of the relaxed bell profiles for both the *Aurelia aurita* and the *Aequorea victoria.*

aurita represented by the dashed line, and the fully contracted bell of the *Aequorea victoria* represented by the dotted line. *Aurelia aurita's* bell deforms along the whole length of the bell, even though the deformation is not uniform and is mainly concentrated at the margin. It is also noticed that the bell extends during the contraction phase which indicates high bell deformation. On the other hand, the *Aequorea victoria's* bell remain almost stationary at the top and starts deforming around 60 % of the bell length. The deformation is mainly concentrated towards the margin of the bell.

To understand the difference in the non-uniform bell deformation of both medusae, the percent bell deformations are measured at five different locations along the length of the bell using the methodology described in Section (4.1). The points are equally spaced in 20 % increments; the first point is positioned at 20 % of the bell length and the last is at 100 %. Figure 4.6 shows the normalized bell deformation of both medusae. It is shown that the *Aequorea victoria* mainly deforms at the margin with minimal deformations at the top. It is

also shown that the *victoria* performs less deformations in the bell compared to the *aurita*.
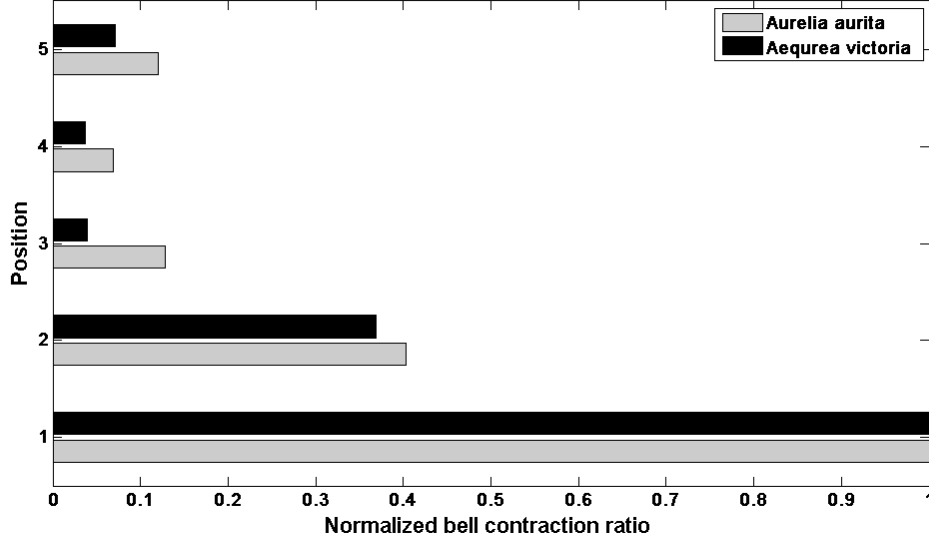
Figure 4.6: This plot shows the bell contraction of both the Aurelia aurita and the Aequorea victroria at five different points along the length of their bells.

Figure 4.7 shows the alterations in the bell shape that are quantified by the fineness ratio, F, defined as follows,

$$F = \frac{h}{d},\tag{4.10}$$

where h is the bell height and d is the bell diameter. The plot shows the instantaneous fineness ratio F(t), that quantifies the variations in bell morphology during the pulsation cycle. The minimum fineness ratio corresponds to the relaxed state of the bell, while the maximum corresponds to the full bell contraction. As shown in the plots the fineness ratio during a swim cycle increases until it reaches a maximum and then decreases again the black solid line corresponds to the *Aurelia aurita*, the minimum fineness ratio is 0.29 while the maximum is 0.58. On the other hand, the dashed line corresponds to the *Aequorea victoria*, where the minimum fineness ratio is 0.42 and the maximum is 0.55. This result is consistent

with the fact time that the *Aurellia aurita* exhibits larger bell deformations. Moreover, the plot shows that the *Aequorea victoria* swims at a slower frequency (1 Hz) since it achieves 3 cycles in around 3 seconds, while the *Aurita* swims at 1.67 Hz since it achieves 3 cycles in almost 1.8 seconds.
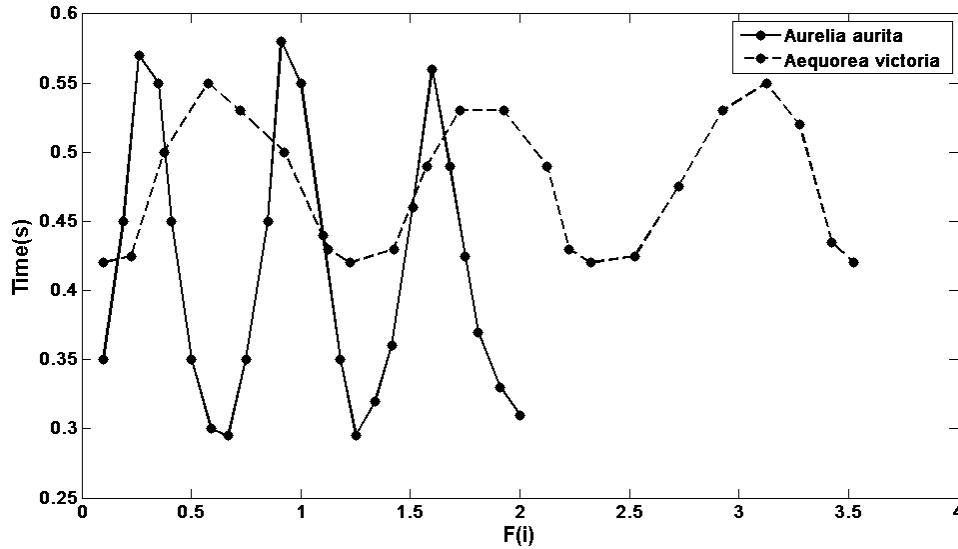
Figure 4.7: Instantaneous bell fineness ratio for the *Aurelia aurita* and the *Aequorea victoria*.

4.1.4   Strain Energy Stored in the Bell

In this section the normalized strain energy in the bell at maximum contraction is computed using the radius of curvature measurements. The reason of this study, is to quantify any potential differences in the actuation requirements of the robot bell. In other terms the lower the strain stored in the bell during the contraction phase, the lower the strain response needed for the IPMC actuators.

The bell profile is treated as a cantilever beam, in a first order approximation and since the

purpose is just to compare the strain energy requirement in each bell. The shape of the bell is spherical and therefore ideally it should be modeled as a shell or spherical membrane. However, assuming the bell is uniform a cross-sectional small section of the bell is isolated and then treated as a cantilever beam. Under these simplifying assumptions the strain energy is defined as the product of the modulus of elasticity E and the square of the strain in the x-direction ϵ_x,

$$U = \frac{1}{2}E{\epsilon_x}^2(z),\tag{4.11}$$

where x and z are the x coordinates and z coordinates, respectively. Therefore, total energy in the x-direction is defined as a follows,

$$U_x = \int_{-z}^{z} \frac{1}{2}E{\epsilon_x}^2\,dz,\tag{4.12}$$

where z is equal to $\frac{t}{2}$ and t is defined as the thickness of the beam. Moreover, the strain in the x-direction of a cantilever beam can be expressed in terms of the curvature of the beam (ρ_x) in the same direction as follows, $\epsilon_x = z\rho_x$. Replacing the strain by its value in Equation 4.12 and integrating results in the following,

$$U_x = \frac{Et^3}{24}{\rho_x}^2.\tag{4.13}$$

In order to compute the total strain energy stored in the beam, 4.13 is integrated with respect to x as shown in the following,

$$U = \int_0^l \frac{Et^3}{24}{\rho_x}^2\,dx,\tag{4.14}$$

where l is the length of the beam. In robotic jellyfish case it is assumed that the bell material is the same, thus the modulus of elasticity is the same, also the thickness of the

bell is assumed to be the same. Therefore, the $\frac{Et^3}{24}$ term is dropped for the purpose of simplification. As a result, the data presented later in this section referred to the $\int_0^l {\rho_x}^2 \, dx$ term which we call by "Non-dimensional strain energy". Figure 4.9 presents the square of
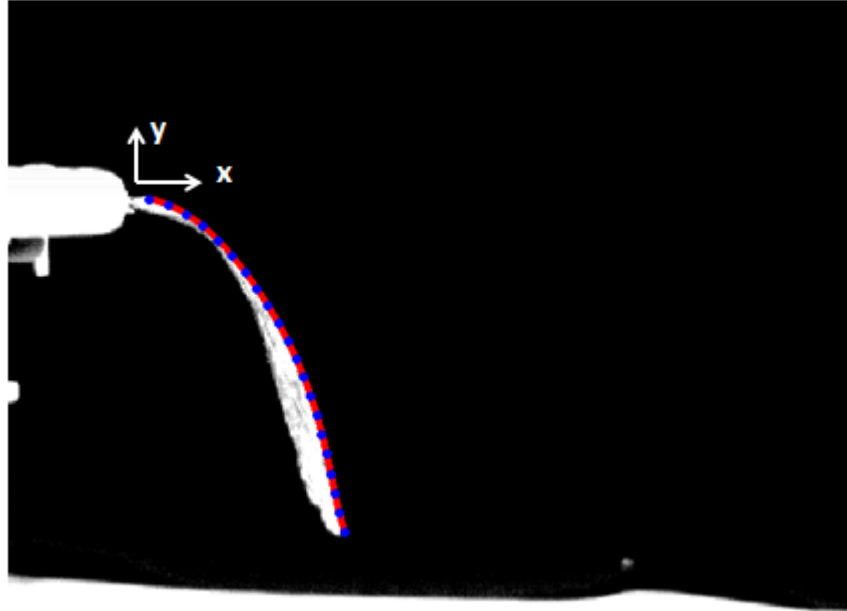
Figure 4.8: Bell profile section represented as a cantilever beam and showing the coordinate axes.

the difference in curvature between the maximum relaxation and contraction states. The *Aurelia aurita* represented by the solid line exhibits a maximum curvature difference at 66.6 % of the length of the bell with a value of $15.58u^{-2}$. On the other hand, the *Aequorea victoria* represented by the dashed line exhibits a maximum curvature of $15.52u^{-2}$ located at 69 % of the length of the bell. Note here that u refers to unit since the bell length is normalized, therefore the values obtained for the curvature difference and the stain energy are dimensionless. Table 4.1 summarizes the curvature results and the overall strain energy stored in the bell of both medusae. The *Aurelia aurita* exhibits an overall stain energy of 3.84 as opposed to 3.53 for the *Aequorea victoria*, which means that for a robot using IPMC
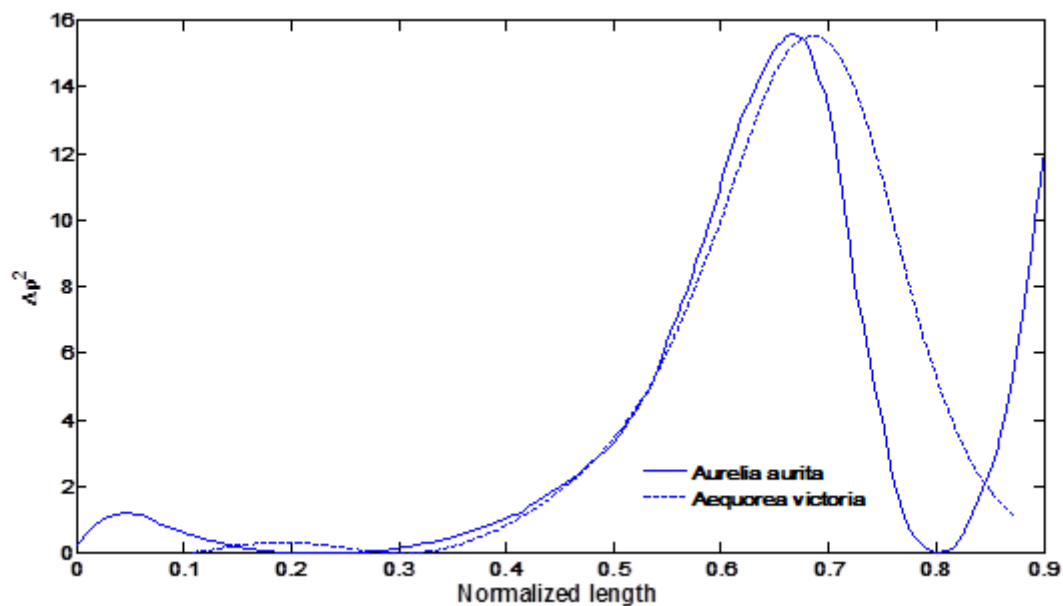
Figure 4.9: The square of the curvature difference at different points along the bell of the *Aequorea victoria* and the *Aurelia aurita*.

as actuators *Aequorea victoria* is a better candidate since less strain energy in the bell is needed when compared to the *Aurelia aurita*.

Table 4.1: A summary of the peak curvature and strain energy results for both medusae.

	$\delta\rho^2(u^{-2})$ peak values	Non-dimensional strain energy	Position
Victoria	15.52	3.53	69.10%
Aurita	15.58	3.84	66.6%

4.2   Bio-inspired Method to Achieve Natural Bell Kinematics and Deformation

As discussed in Chapter 1 and in the previous section, the bell of oblate species deform in a non-uniform way. The top part of the bell exhibits minimal deformations while larger deformations are concentrated toward the margin of the bell. This section focuses on the design of a bio-inspired bell that mimics the morphology and kinematics of the natural jellyfish. In the first part of this section, the experimental setup and characterization of the biomimetic are discussed while the results are presented and analyzed in the second part.

4.2.1   Experimental Method and Set Up

The first step in conducting these experiments is to fabricate a test structure that would mimic the morphology of the jellyfish bell and enable testing of multiple actuator configurations. The experimental apparatus that is developed consists of a central hub, a single IPMC actuator, a one-eighth section of a symmetric bell, and a stage that enables changing the position (x and y) of the actuator and the angle at which it is located underneath the bell.

The hub consists of two circular halves made from ABS plastic and printed using a rapid prototyping machine. Each part have eight radially distributed gold electrode pads that provide mechanical and electrical support for the IPMC actuators. The bell section is made from polyolefin film that is able to hold the shape of the biomimetic bell while maintaining low stiffness which is essential for an IPMC-based design. The stage is made from a rectangular plexiglass piece that has equally spaced 3 mm holes. These holes will serve in moving the stage and thus the actuator in the y-direction on a threaded tube and also the stage is able

to move in the x-direction, to hold it in position two 3 mm nuts are used. These parts are shown in Figure 4.10.
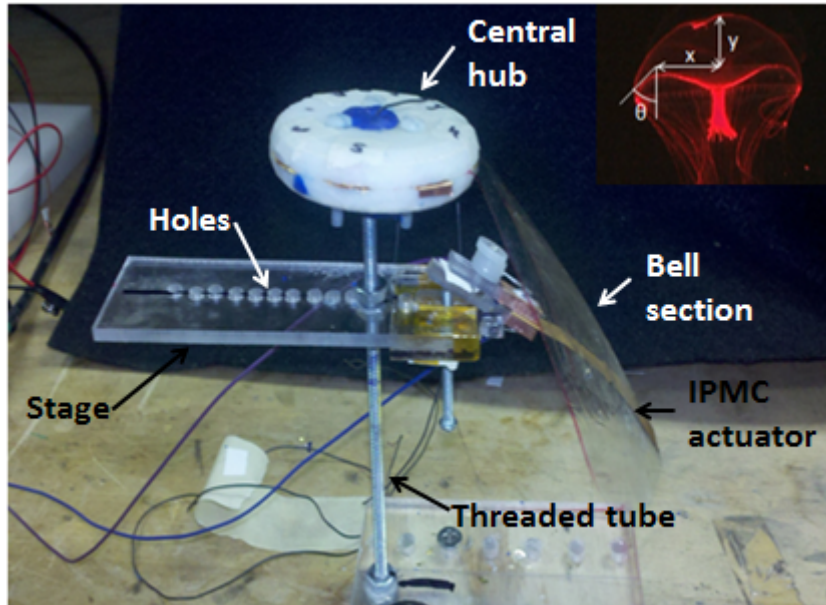
Figure 4.10: The assembled experimental setup, at the top right is a picture of the actual *Aequorea victoria* also showing what it is meant by x,y and .

The experiments are designed in a way to understand the effect of varying the position and the size of the actuator on the bell deformation. Therefore, three different actuators with similar peak to peak strains percent are used in this set of experiments. The actuators are of different sizes: a small actuator $(4.5cm \times 0.5cm)$, a medium actuator $(5cm \times 0.8cm)$ and a large actuator $(6.5cm \times 1.0cm)$. Varying the actuator surface area by varying its size will enable the study of the effect of the actuator size on the actuation performance of the bell and also on the power consumption. Taguchi's method [34] is used in order to design the experiment, having three different parameters (x, y, θ) with four different levels each. Table 4.2 shows the distribution of sixteen experiments for each actuator where L refers to level.

Table 4.2: Experiment distribution according to Taguchi's method having three parameters with four levels each.

Experiment	y	x	θ
1	L1	L1	L1
2	L1	L2	L2
3	L1	L3	L3
4	L1	L4	L4
5	L2	L1	L2
6	L2	L2	L2
7	L2	L3	L4
8	L2	L4	L3
9	L3	L1	L3
10	L3	L2	L4
11	L3	L3	L1
12	L3	L4	L2
13	L4	L1	L4
14	L4	L2	L3
15	L4	L3	L2
16	L4	L4	L1

4.2.2   Experimental Results

The results of a total of 48 experiments are summarized in Figure 4.11. These results are classified under three different categories: Far, Fair and Close compared to the actual medusa's data. Specifically, the data of interest are the total non-dimensional strain energy stored in the bell and the location of the point of inflection (i.e. the point of maximum curvature difference).

Most of the results fell under the "Far" category (Figure 4.11), since the deformation of the ionic polymer metal composites is bulk and thus hard to control and makes it difficult to attain the exact shape of the medusa's bell. However, some experiments fell under the "Fair" category since they exhibited reasonable results when compared to the actual animal.

| Experiment | Actuator | | |
	Small	Medium	Large
	1	1	1
	2	2	2
	3	3	3
	4	4	4
	5	5	5
	6	6	6
	7	7	7
	8	8	8
	9	9	9
	10	10	10
	11	11	11
	12	12	12
	13	13	13
	14	14	14
	15	15	15
	16	16	16

Far
Fair
Close

Figure 4.11: Summary of the bell profile experiments for a total of 48 experiments.

On the other hand, the best results are the ones of experiments 4,5 and 6 when the medium-sized actuator is used. These results are summarized in Table 4.3 and show fairly close deformation to those of the actual jellyfishes, with maximum peak curvatures of 7,10 ,and 10 for experiments 4,5 ,and 6 respectively. The locations of the maximum peak curvature for these experiments (65 %) are to large extent close to the real jellyfish. These results are promising because they are close match to the results of the natural medusae. Note that the IPMC actuator exhibit bulk deformation and thus controlling it to achieve exacts bell deformations needs higher fabrication and patterning techniques.

Another interesting result of these experiments is related to the power consumption of the actuators. Due to the reduction in the size of the actuators in all three experiments, the power consumption is reduced. Figure 4.12 shows the power consumption results of the large

Table 4.3: Summary of the peak curvature and strain results of the best 3 experiments.

Experiment	$\Delta\rho^2(u^{-2})$ peak values	Non-dimensional strain energy	Position
4	7	4	64 %
5	10	10	65 %
6	10	10	65 %

and medium actuators. It is shown that the power is reduced by 40 % when the size of the actuator is reduced by   39 % from 6.5 cm^2 (large actuator) to 4.0 cm^2 (medium actuator).
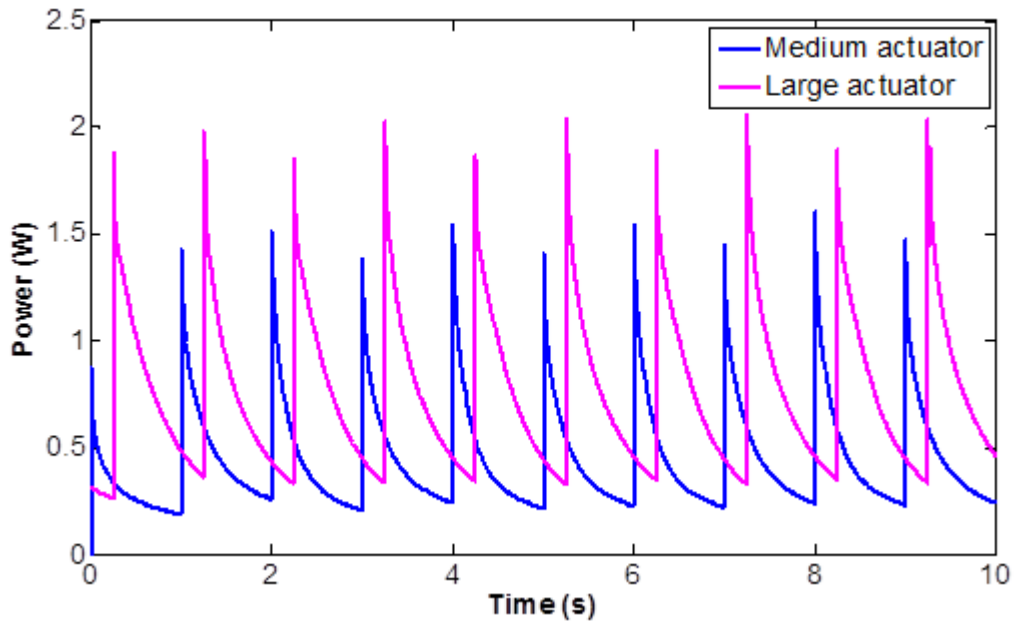

Figure 4.12: Power consumption results comparison between the large and the medium actuators.

4.3   Chapter Summary and Conclusions

In this chapter the analysis and design of a biomimetic bell are presented. Bell kinematics determine the propulsion technique and thus affect the swimming speed and efficiency of the jellyfish. Therefore, the "Oblate" species are more efficient since they depend on rowing propulsion technique caused by the non-uniform bell deformations for propulsion.

A comparative study on the bell kinematics and morphology of the *Aequorea victoria* and the *Aurelia aurita* is also presented. This study shows that the geometry of the *Aequorea victoria* is more suitable for an IPMC-based robot since it has a more spherical shape as opposed to the flattened shape of the *Aurelia aurita*. This conclusion was based on the results of the first generation robot that demonstrated that the smaller the angle the IPMC actuator makes with the vertical, the better the actuation performance. On the other hand, this study also proves that the strain energy stored in the *Aequorea victoria's* bell during the contraction phase is lower than the energy stored in the *Aurelia aurita's* bell. This result is important since less strain energy in the bell means that less strain energy for the actuators is needed.

On a different level a series of experiments were conducted in order to recreate the bell deformation the *Aequorea victoria*. Three different actuators each having a different size were used in the experiments. The results show that three different actuator configurations resulted in a deformation similar to the natural jellyfish in terms on maximum deformation, point if deflection, and strain energy. These configurations were achieved using a medium sized actuator (5 cm × 0.8 cm) which resulted in a power reduction of 40% associated with the reduction in size the original actuator used in the first two generations.

Chapter 5

Design of a Biomimetic Robotic Jellyfish

5.1 Initial Attempt and Proof of Concept Trial

This section presents the design and development of a jellyfish robot using IPMC actuators for propulsion. This first generation are investigated serves as a proof of concept and initial attempt to test the swimming capability of an IPMC-based robot. Several parameters including the input waveform to the actuators, the shape of the bell and material of the bell. The design parameters are discussed in the first part of this section, while the free swimming results and power consumption are presented in the second part.

5.1.1   Design Parameters

Two robotic jellyfishes are built and both served as a proof of concept. These robots are powered using water-based IPMC actuators. The first robot is developed in order to demonstrate the ability of using ionic polymer metal composite actuators as a propulsion mechanism. It consists of an acrylic base, an air filled ping-pong ball to control buoyancy, a polyethylene thin film and IPMC actuators. The acrylic base (Figure 5.1 (a)) is composed of eight ribs each containing a gold electrode. The gold electrodes are connected in parallel and serve as mechanical support and electrical connection to the actuators which are sandwiched and held in a cantilever configuration. The ping pong ball attached at the top of the acrylic base helps to control the buoyancy of the robot. However, in order to make the jellyfish robot neutrally buoyant in water, counter weights are hanged on the lower part of the base.

The polyethylene film is glued to the acrylic base of the robot and attaches to the actuators through polyethylene sleeves ($1cm \times 5cm$) that in turn are attached to the bell (Figure 5.1 (b)). The IPMC actuators are attached from one side to the acrylic base and from the other side they are inserted inside the sleeves. To reduce the friction between the actuators and the sleeves small plastic pieces are inserted into the sleeves.

Finally, it was shown from different attempts by other research groups that flaps at the margin of the bell tend to improve the swimming speed. Therefore, in the last step flaps are attached to the end of the IPMC actuators. The flaps have a rectangular shape (4 cm$\times$ 3 cm) and are made from a thin sheet of DRAGON SKIN^{TM} silicon. The flaps are then glued to the margin of the polyethylene bell.

The first version of the proof of concept robot proved to be heavy and not biomimetic. Therefore , a second version is built where the robot is redesigned to become more biomimetic
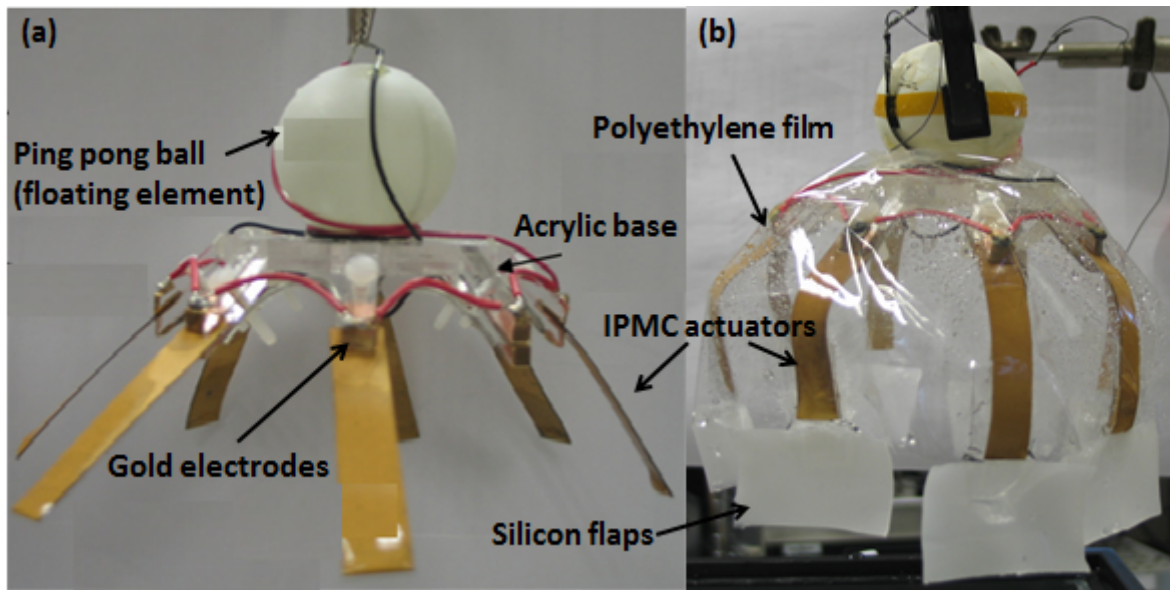
Figure 5.1: (a) Photographic picture showing the acrylic base and the floating element (b) photographic picture showing the assembled jellyfish robot.

and lighter. The second version is distinguished by first, its shape which mimics the *Aurelia aurita* jellyfish and second, by its light weight. The maximum diameter of this robot is 16.5 cm with a depth of 5 cm. The bell is spin coated in a biomimetic 3D printed mold, using 40 grams of the DRAGON SKIN^{TM} silicon (Figure 5.2).

The floating element in this version is a Styrofoam cylinder of 4.5 cm diameter and 0.7 cm thickness. The acrylic base is replaced by a gold plated acrylic ring which is glued to the floating part and the silicon bell together. Another gold plated acrylic ring is screwed to the top electrode supporting eight IPMC actuators. The 1 cm × 6.5 cm actuators are placed in a cantilever configuration and sleeves similar to the ones used in the first version are glued to the bell to hold them on the other side.
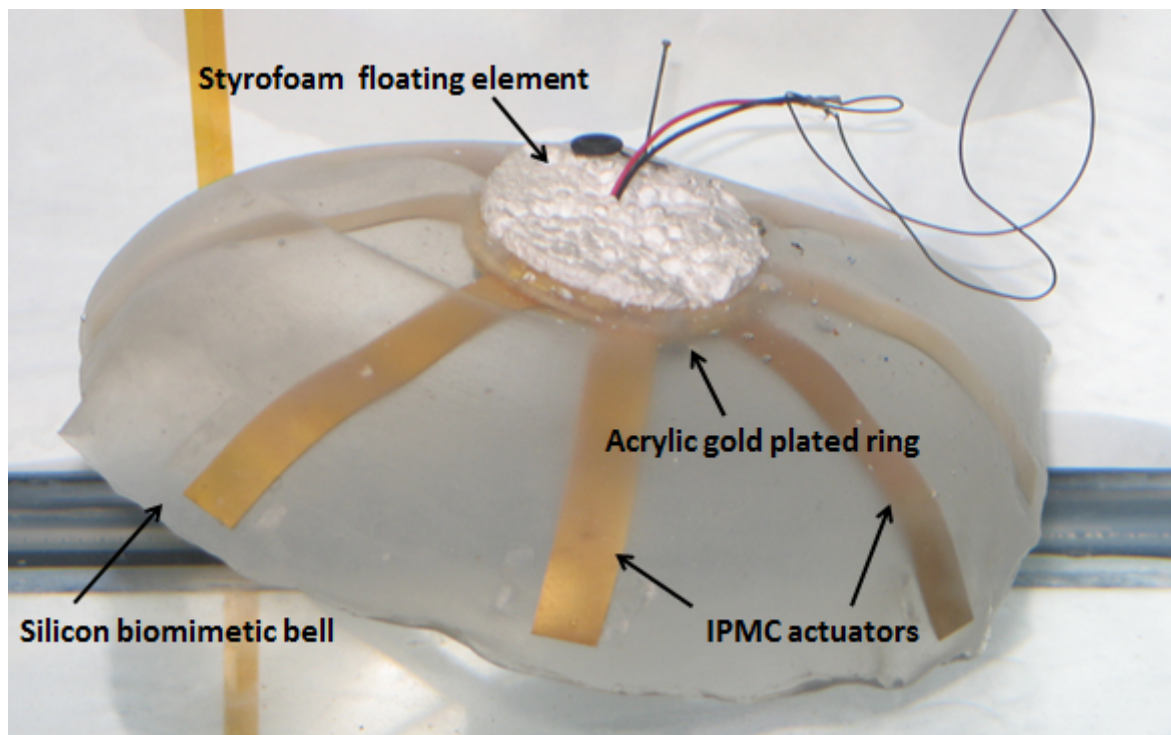
Figure 5.2: Photographic picture of the second version of the IPMC jellyfish robot showing the biomimetic silicon bell.

5.1.2   Characterization and Results

The characterization process of the robot is explained in details in Chapter 2. Substantially, the robots are characterized in a water filled aquarium (40 cm × 20 cm × 26 cm). A D-Space data acquisition system is used to apply the signal waveform voltage, and also in order to record the current consumed by the robot and using a non-inverting op-amp circuit. The free swimming of the robot is recorded using a high speed camera, the videos are processed later using a motion trace software.

Several waveforms such as sine, sawtooth, and square waveforms are used and optimized in order to maximize the acceleration and velocity of the robot. The square wave signal proved to be the most convenient which is also consistent with the biological jellyfish since

the power and relaxation strokes can be described as square wave. Figure 5.3(a) shows a typical square waveform applied to the robot while Figure 5.3 (b) and (c) show the current and power consumption respectively. The applied potential in 4 V peak-to-peak and varies between +2 V (power stroke) and -2 V (relaxation stroke), while the frequency and duty cycle are changed and optimized. The optimization of the waveform is done by varying the duration of the power stroke (contraction phase) to the duration relaxation phase, while the motion of the robot is recorded for each case.
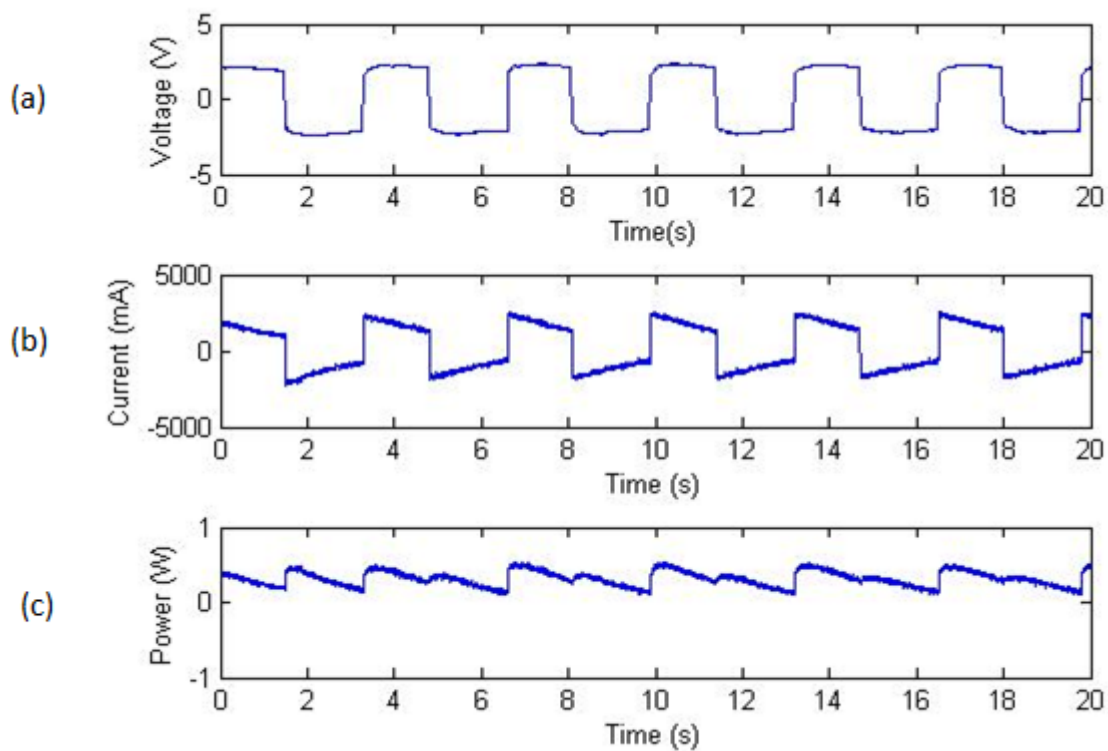

Figure 5.3: (a) The input voltage used to actuate the robotic jellyfish, (b) the current consumption of the robotic jellyfish, and (c) the power consumption of the robotic jellyfish.

Figure 5.4 shows the free swimming results of 17 different trials each having different frequency and duty cycle. Figure 5.6 presents a third order curve fit of the data presented in
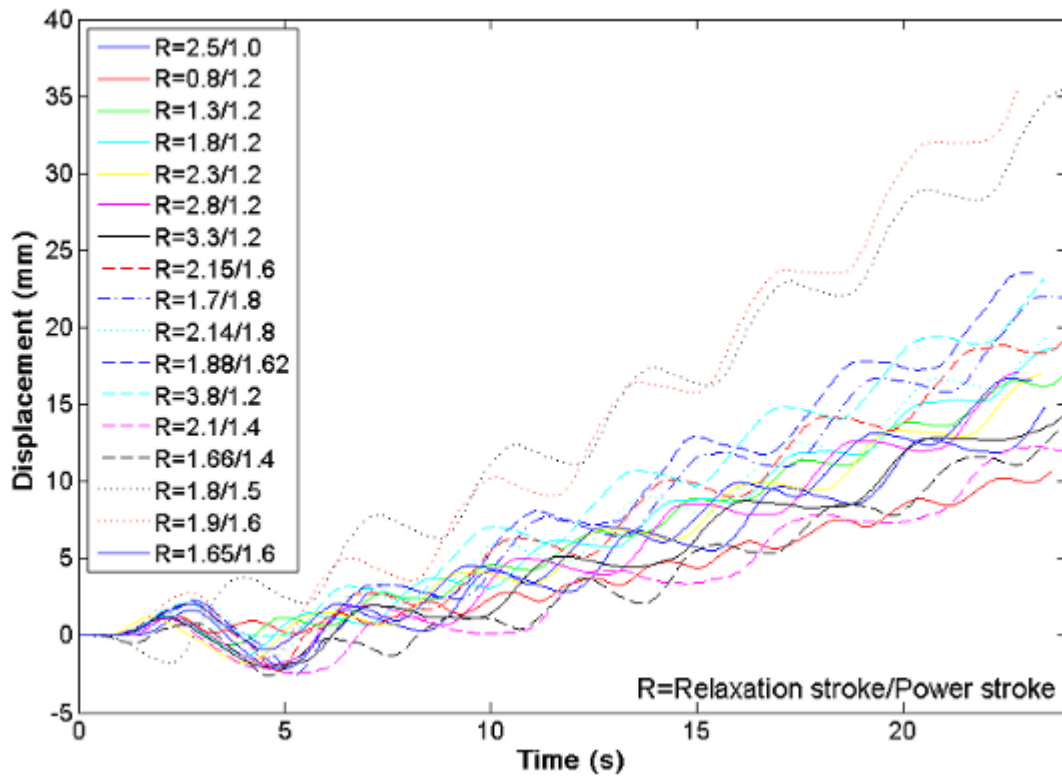
Figure 5.4: The displacement curves of the robot as the ratio of the Relaxation stroke to the Power stroke is varying.

Figure 5.4 which represent the average displacement of the robot in time. Figure 5.6 also shows the slope of the time at 10 seconds which is considered to be steady state velocity. These results show that the 1.9 seconds for relaxation stroke and the 1.6 seconds for the power stroke signal, is the optimal waveform in this case. To elaborate more on the results, the best waveform dynamic response is shown in Figure 5.7 (a) through (f). The velocity results show the peak velocity attained is approximately 6 mm/s, while the average speed is around 2 mm/s. The swimming performance of the robot is also compared to the natural jellyfish performance, and the fineness ratio is used for this purpose. Figure 5.8 show the fineness ratio of the robot as well as of the *Aurelia aurita*. It can be concluded that the
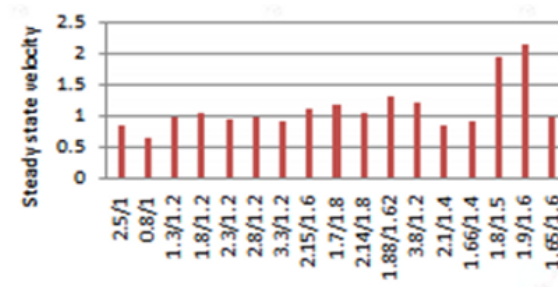
Figure 5.5: The average swimming speed as function o relaxation to power stroke ratio.

robot operates at a lower frequency as compared to the natural jellyfish, even though the ratio of the relaxation stroke to the power stroke is similar. This robot served as a proof of concept and it proves that a robot based on IPMC actuators can swim. The maximum average speed attained is 2 mm/s with a power consumption of 3.2 W.

5.2   First Generation Mimicking the *Aurelia aurita*

This section presents the design, fabrication, and characterization of a robotic jellyfish that mimics the shape and swimming style of the *Aurelia aurita*. The robot uses ionic polymer metal composites as actuators for propulsion. The choice of the *Aurelia aurita* is based on its high swimming efficiency and since its morphology and swimming behavior are will understood and described in the literature. The following subsections focus on the bio-inspired design and development of the robot. First, the design parameters and fabrication processes are discussed. In the second part the characterization process and free-swimming results are presented and discussed.
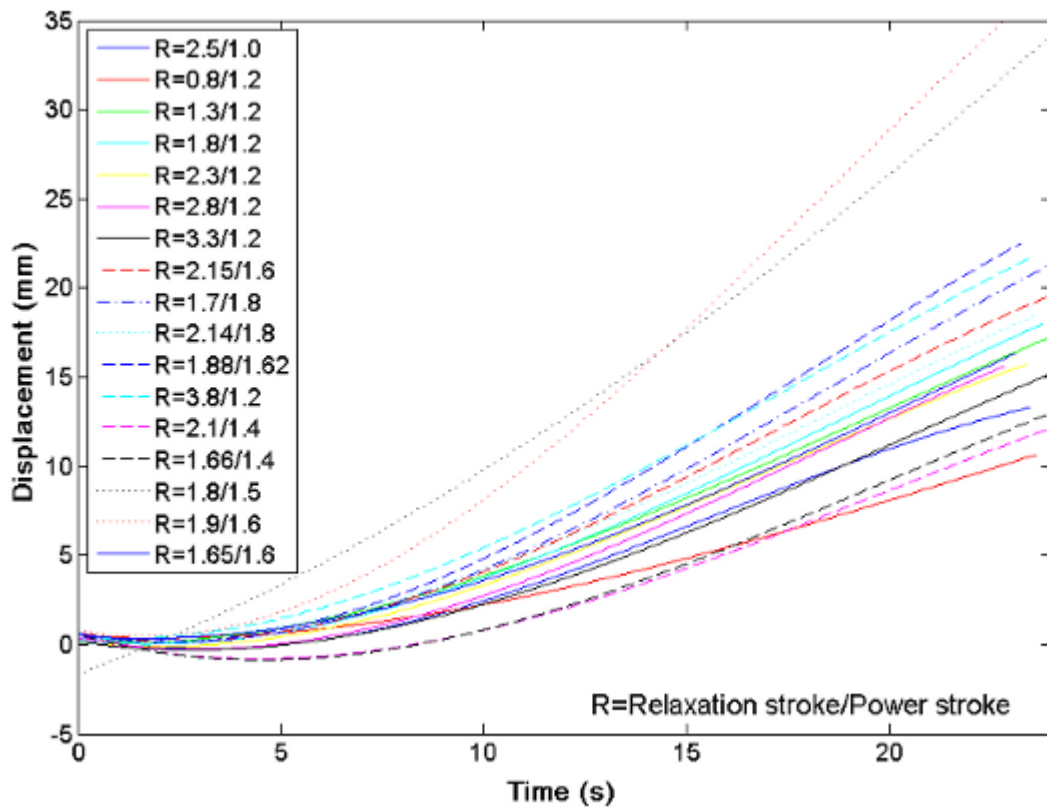
Figure 5.6: A curve-fit of the average displacement.

5.2.1   Design Parameters and Fabrication Process

The robot consists of three parts: a central hub, the IPMC actuators, and a flexible biomimetic bell. The central hub replaced the acrylic base used in the previous generation. The hub is composed of two lightweight plastic circular halves, each having eight radially distributed gold electrodes. The gold electrodes serve as a mechanical support and provide electrical connection to the actuator that are attached in a cantilever configuration. The hub in made of ABS plastic and is printed using a rapid prototyping machine. The electrodes are made with gold foil (*Arrow Springs, 23 kt, 65 g/m*) and are connected in parallel Figure 5.9 (b) and (d). Gold is used for its high conductivity and resistivity to corrosion. Figure 5.9
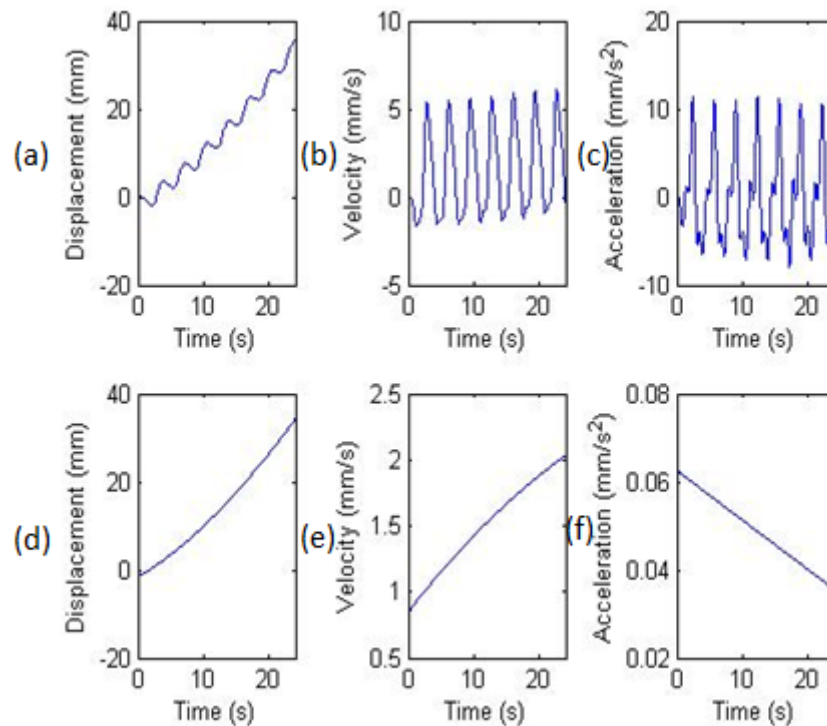
Figure 5.7: (a) Displacement, (b) velocity, and (c) acceleration of the robot due to square waveform of relaxation stroke of 1.9s and power stroke of 1.6s. Also presented are the average curves of (d) displacement, (e) velocity, and (f) acceleration.

shows the CAD models of the hub along with photographic pictures of the printed pieces. The electrical connection is chosen such as the actuators are actuated simultaneously.

The biomimetic, flexible bell is made from heat shrinkable polyolefin film. Polyolefin is adapted in this design for its low stiffness and shape-holding ability, which are essential for an IPMC-based design especially that IPMCs are known by their low blocking force. A biomimetic mold is used to shape the bell of the robot. The mold mimics the geometry of the *Aurelia aurita* jellyfish. The dimensions and coordinates of the mold profile are taken from the digitized *Aurelia aurita* bell profile discussed in Chapter 3. The coordinates are then imported to the CAD software Unigraphics NX7.0, where the mold is modeled in addition
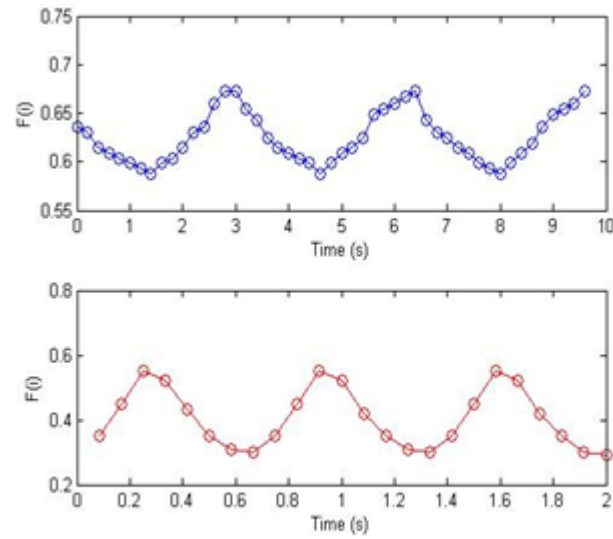
Figure 5.8: Top graph showing the instantaneous fineness ratio of the jellyfish robot while bottom graph shows the instantaneous fineness ratio of the *Aurelia aurita*.

to different parts that makes the robot.

Finally, eight IPMC actuators ($6.5cm \times 1cm$ each) are inserted between the two hub halves and extend radially out from the hub in a cantilever configuration. The free end of each actuator is held by a horizontal sleeve made from rectangular polyolefin films and attached at the inner side of the bell.

The final weight of the robot is approximately 14 grams as opposed to 42 grams for the previous generation. The maximum diameter of the bell is 16.4 cm with a depth of 5 cm (Table 5.1). Figure shows the assembled biomimetic jellyfish robot.
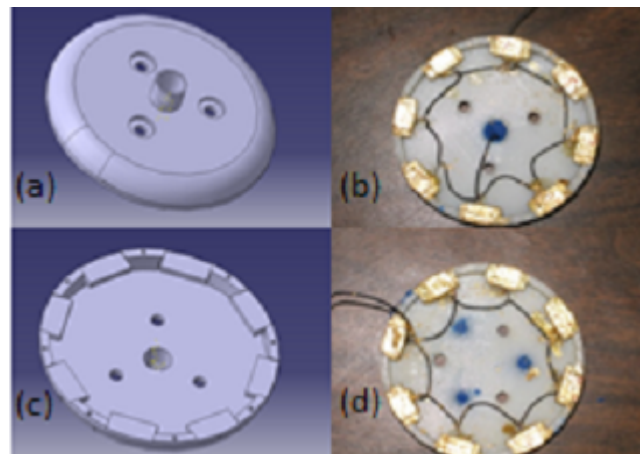
Figure 5.9: (a-c) CAD model of the top and bottom halves of the hub . (b-d) Top and bottom halves of the hub with applied gold electrode layers and the wired connections.

5.2.2   Free-Swimming Results

The ability of the *Aurelia aurita* jellyfish robot to swim freely is studied as a function of two design and operation parameters: the input voltage waveform and the bell geometry.

Input Voltage Waveform Effect

The input voltage waveform to the robotic jellyfish is shown in Figure 5.10. The signal consists of a square wave with varying duty cycles used when testing the swimming behavior of the robot. The voltage amplitude of the signal is held constant at 2V (4V peak-to-peak), and the duty cycle of the square wave was varied between 30 % and 50 % in a 5 % increment. The current consumption (Figure 5.10 (b)) is also measured and recorded for the input voltage signal shown in Figure 5.10(a).

The swimming speed and power consumption depended on the applied voltage waveform. As the duty cycle is varied, the net motion of the robot changes. Figure 5.11 shows the

Table 5.1: A summary of the robot dimensions, materials used and fabrication methods.

	Design	Dimensions	Material
Hub	Two-piece circular hub with 8 radially-spaced gold covered electrode surfaces	$d = 5cm, h = 1cm, W = 11g$	ABS plastic, 3D printed
Bell	modeled after *Aurelia aurita*	$d = 16.4cm, h = 5cm, F\ 3$	Polyolefin, $t = 50\mu m$
Actuators	Cantilevered, beam-type	$l = 6.5cm, w = 1cm, t = 300\mu m$	water-based IPMC

resulting vertical motion of the robot during a 30 seconds actuation period for two specific duty cycles at 2V.

Both plots exhibit an oscillatory motion corresponding to the frequency of the applied waveform (0.5 Hz). The 30 % duty cycle cycle produced more than a factor of two increase in total displacement during the test, with an average slope of 1.5 mm/s and an average power consumption of 3.5 W. This study demonstrates that an unbalanced square is required in order to increase the swimming speed of the robot.

Bell Geometry Effect

As previously mentioned IPMC actuators have relatively low stiffness and are known for their low blocking force which will reduce the thrust. This constraint is overcome by using low-stiffness bell material, however radial cuts are introduced to the bell which enables fortuning the bending stiffness of the molded bell. The cuts are positioned between the actuators and extend from the bell margin toward the central hub.
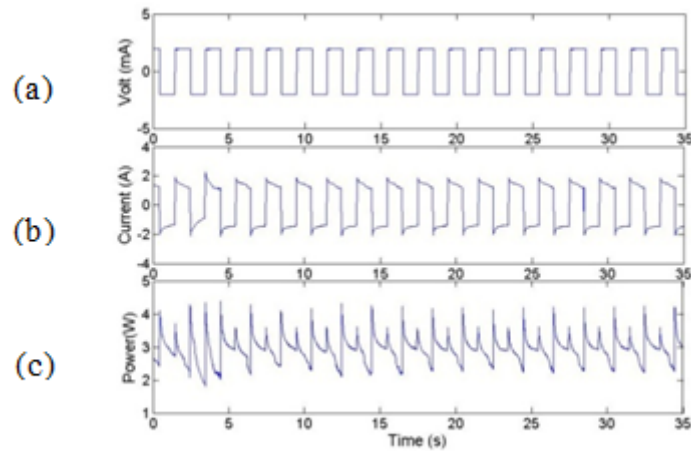
Figure 5.10: (a) The input voltage used to actuate the robotic jellyfish, (b) the current consumption of the robotic jellyfish, and (c) the power consumption of the robotic jellyfish.

Three sets of swimming tests are performed to understand the effect of bell geometry and stiffness: a bell with no cuts, a bell with cuts extending half-way, and a bell featuring all-the-way cuts in to the hub.

Figure 5.12 shows vertical displacements of the robot having these three different bell geometries. When no cuts are introduced to the bell the robot remains stationary due to the softness of the actuators. Introducing the cuts improved the swimming performance of the robot.

The robot swam faster with an oscillation frequency (0.5 Hz) similar to the uncut bell, when half-way cuts are introduced. However, increasing the length of the cuts does not results in an increase in swimming speed, but it does change the swimming oscillation frequency.
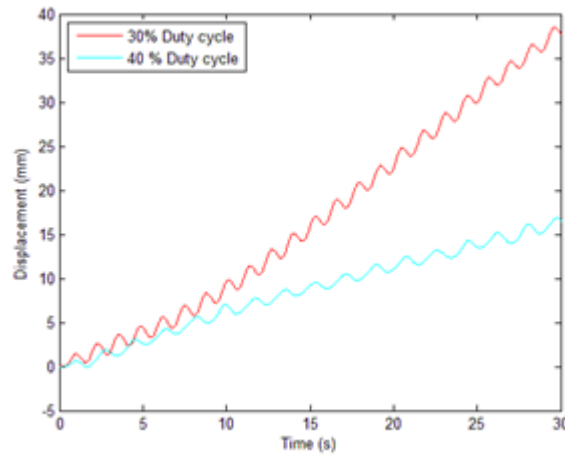
Figure 5.11: The vertical displacement of the jellyfish versus duty cycle for an applied square wave of 2V and 0.5 Hz.

Design Assessment

The rates of the change of the shape, or the fineness ratios of the robot and natural jellyfish are compared. Figure 5.13 shows the fineness ratio change in function of time, for the natural jellyfish is represented in red while the robot in blue. It is obvious that the natural species swims at a higher frequency compared to the robot. This can be associated with the slow response rate property of IMPC actuators.

Moreover, it is also shown that the natural *Aurelia aurita* contracts more where its bell fineness ratio ranges from 0.29 to 0.57 while the robot's ranges from 0.29 to 0.32.

From these results one can conclude that the properties of the *Aurelia aurita* might not be the most appropriate to serve as a model system for an IPMC based robot.
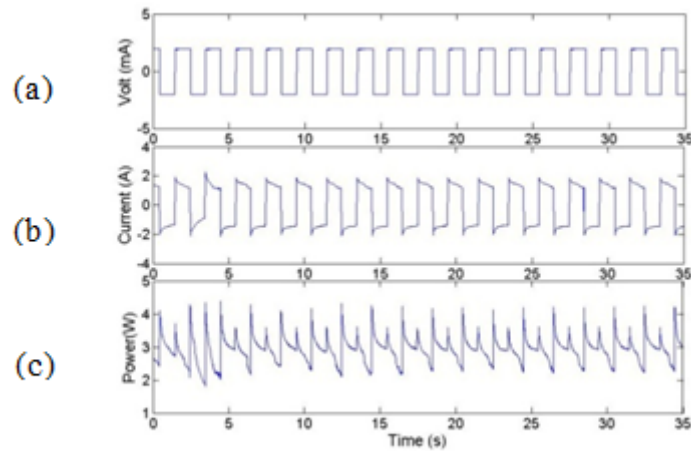
Figure 5.12: This plot is showing the displacement of the robot for different bell geometries.

5.3   Bio-mimetic Design Based on *Aequorea victoria* as a Model System

5.3.1   Design Parameters

The results in Chapter 4 describe the motivation and approach for focusing on the *Aequorea victoria* as a model system for a bio-inspired robotic jellyfish based on IPMC actuators. This specific species swims at a slower frequency compared to other oblate species and contract minimally with the smallest fineness ratio range compared to other medusae. These properties fit the mechanical properties of the IPMC actuators.

The *Aequorea victoria* jellyfish robot consists of four different parts: a central hub, eight radially distributed spars, a stage, the IPMC actuators, and a flexible bell. The central hub is composed of two lightweight plastic parts. The top half has a t-shape where the horizontal disc represents the hub and the vertical tube represents the part at which the stage will be
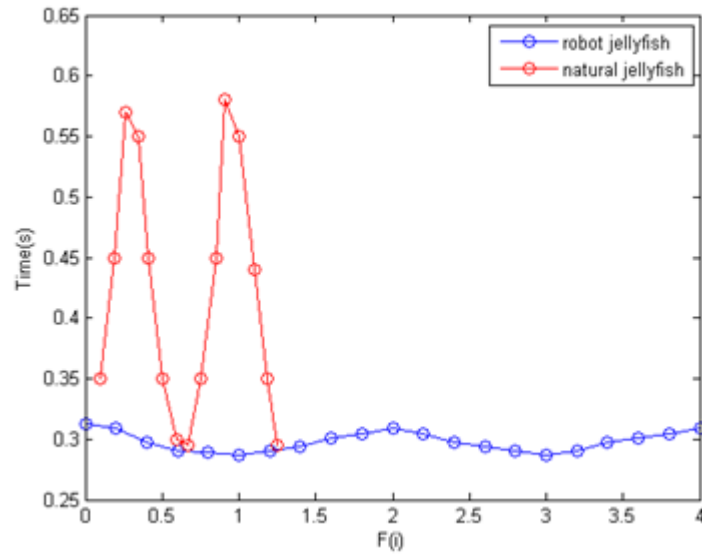
Figure 5.13: This plot showing the fineness ratio versus time for both the natural and robotic jellyfishes.

attached. The bottom part of the hub is a simple cylindrical piece use for support. Both parts (Figure 5.14) are printed using a rapid prototyping machine and are made from ABS plastic material.

The eight radially distribute spars (Figure 5.15 (a)) extend from the central hub to 69% of the synthetic bell (natural species bell inflection point), in order to keep the top part stationary during the contraction phase. The spars also add stability to the submerged robot.

The stage is a dynamic central body that serve as a mechanical support to the IPMC actuators. It consists of a main part and eight similar clamps. Figure 5.15 (b) shows the CAD models of the assembled structure. The clamps that also serve for electrical connectors to the actuators through gold electrodes located at the tip of each clamp. The electrodes are fabricated with gold foil (Arrow Springs, 23 kt, 65 g/m) and are wired such that the contacts on the lower and upper clamps are wired in parallel as illustrated in Figure 5.3.1. This
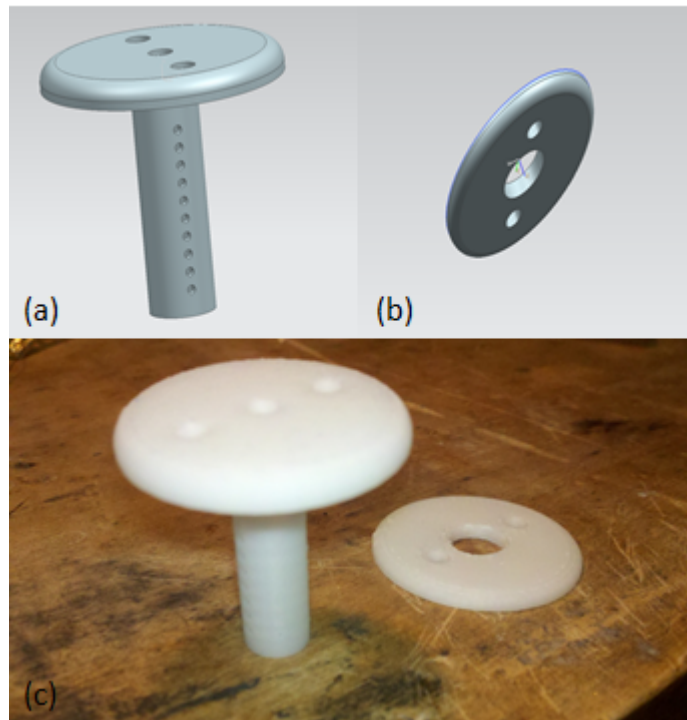
Figure 5.14: (a) CAD model of the t-shaped top part it the hub, (b) CAD model of the bottom part of the hub, (c) 3D printed parts of the central hub.

electrical arrangement is chosen such that all IPMC actuators are actuated simultaneously.

The lightweight, flexible bell is made from polyolefin film that is chosen for its combination of shape-holding capability and low stiffness. A 3D printed biomimetic mold (Figure 5.17) mimicking the *Aequorea victoria* is used to shape the robot bell.

Finally, IPMC actuators (5 cm × 0.8 cm each) are sandwiched between the two halves of the equidistant clamps and extend radially outward from the stage. The free end of each actuator is attached to the bell by a horizontal sleeve around the bell margin.

The final robot weighs around 20 grams and has an overall diameter of 15 cm and a height of 5.8 cm. The assembled biomimetc jellyfish robot is shown in Figure 5.18.
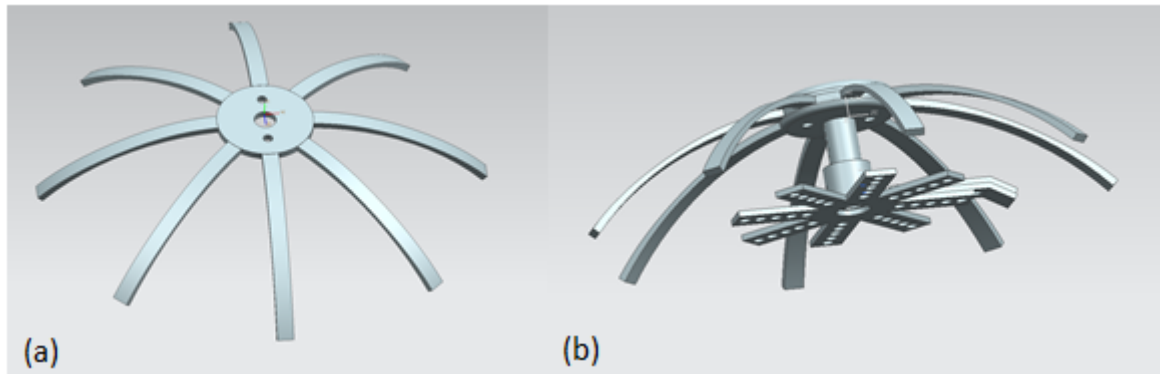
Figure 5.15: (a) CAD model of eight radially distributes spars, (b) CAD model of the assembled parts that make the jellyfish robot.

5.3.2   Free Swimming Average Speed and Power Consumption

The robot is actuated by four actuators for the first set of experiments and eight for the second set. For each set of experiments the position of the actuators was varied in the y-direction between 1.5 cm and 2 cm. At each actuator position, two bell configurations were tested (full bell and half way cut bell), and for each configuration, a square waveform voltage is applied at different frequencies and with different duty cycles.

Figure 5.19 (a) shows an example of an input voltage waveform to the robot. A particular signal which consisted of a square wave with different duty cycles was used when testing the swimming ability of the robot. In this study, the voltage amplitude was held constant at 2V (4V peak-to-peak), and the duty cycle of the square wave was varied from 30% to 50%. The current consumption of the robotic jellyfish for the applied voltage shown in Figure 5.19 (a) was also measured and is shown in Figure 5.19 (b). The power consumption is thus computed using measured values of the applied voltages and resulting currents. The average power consumption for the jellyfish was 0.7 W when four actuators were used and 1.14 W when eight actuators used. Notice that both the current and power consumption varied with
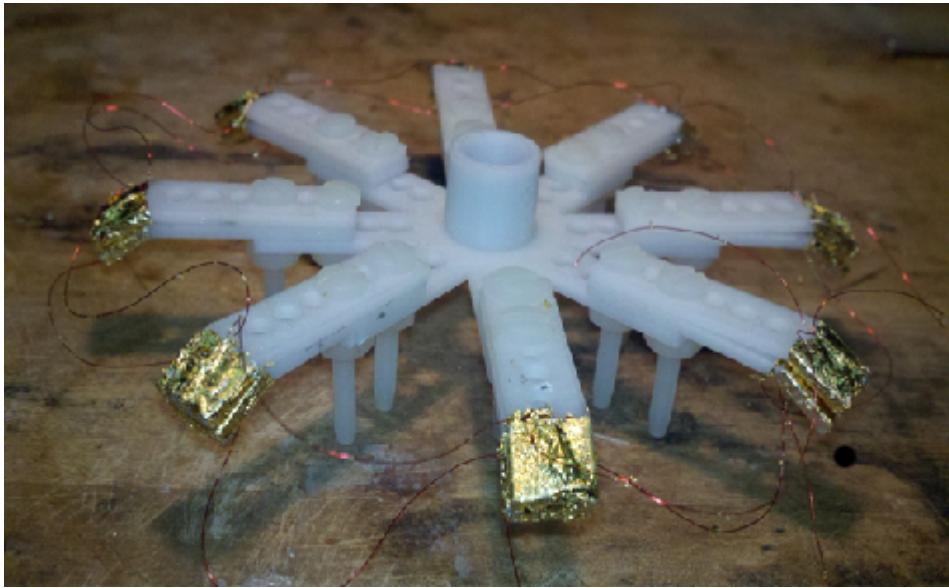
Figure 5.16: A photograph showing the central stage, the clamps and the electrical connections.

the variation of the duty cycle. The resulting motion of the jellyfish also depended on the applied voltage waveform.

Our results demonstrated that the net motion of the robot changed as the duty cycle was varied. Figure 5.20 shows a 3D plot of the velocity of the jellyfish in function of both the frequency and the duty cycle. Akle, et al also demonstrated that an asymmetric square wave (45% duty cycle) achieved the maximum swimming speed with the first generation robot. One limitation of using IPMC materials for actuating the jellyfish is that their relatively low stiffness and blocked force (0.74 N/m and 20 MPa, respectively) limits thrust. This constraint was overcome by using a bell material that is highly flexible but which can also maintain the undeformed bell geometry. Using a heat-shrinkable polyolefin film, a lightweight flexible bell was molded to mimic the shape of Aequorea victoria jellyfish.

As a method for reducing the bending stiffness of the molded bell, radial cuts positioned between actuators and extending from the outer perimeter in toward the hub are introduced.
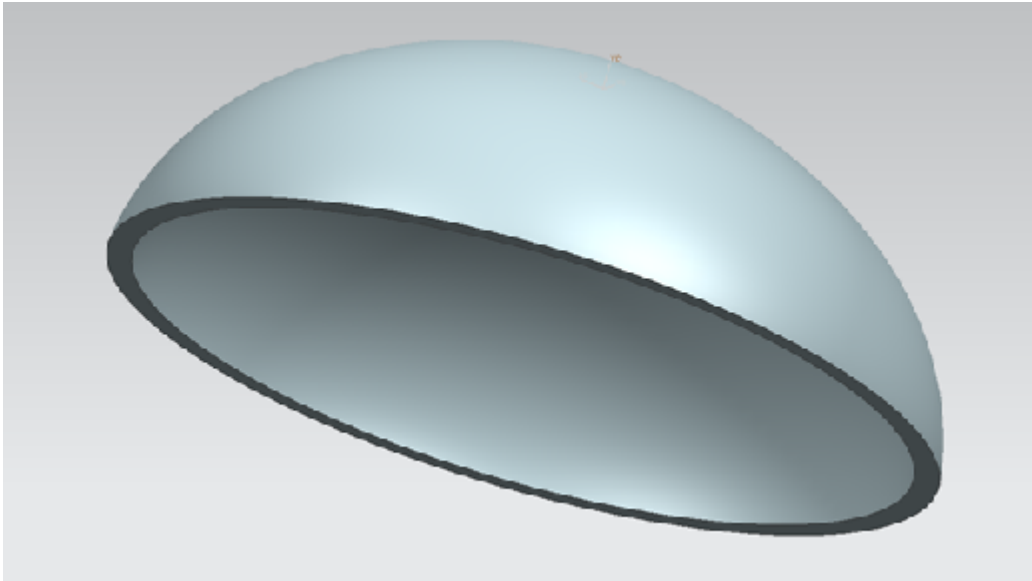
Figure 5.17: CAD model of the biomimetic mold used in fabricating the robot bell.

A similar approach was used by Villanueva, et al for increasing the swimming speed and actuation profile of the SMA-actuated biomimetic jellyfish. Two sets of swimming tests were performed to understand this effect of bell geometry and stiffness: a bell with no cut and a bell with cuts that extend half-way from the outer edge to the hub. Figure 5.21 shows the vertical displacement of the jellyfish robot during a 30 s actuation period for four different configurations of the robot at 2V. The traces exhibit an oscillatory motion corresponding to the frequency of the applied waveform and demonstrate that the jellyfish swam upwards. When no cuts are introduced to the bell the robot swims at slower velocities due to the increase in mechanical resistance of the bell. When the cuts are introduced to the bell, the performance of the robot improved. When half-way cuts are introduced, the robot swam faster with oscillation frequency similar to the uncut bell. Figure 5.21 also shows the results for two different positions of the stage at 1.5 cm and 2 cm from the hub. The results shown in Table 5.2 also show that the robot swims faster when the stage is positioned at 1.5 cm. Finally Figure 5.21 also shows the vertical displacement for the robot when eight actuators

Figure 5.18: A picture of the assembled jellyfish robot.

are used. This robot swam at a speed equal to 1.5 mm/s and consumed 1.14 W.

Table 5.2: A summary of the swimming frequency, duty cycle and speed of the robot along with the power consumption for the four different configurations.

	Bell	Frequency (Hz)	Duty cycle (%)	Average speed (mm/s)	Average power (W)
1.5 cm	Half-cuts	0.67	46.67	0.77	0.7
	no-cuts	0.67	33.33	0.72	0.65
2.0 cm	Half-cuts	0.5	25	0.4	0.55
	no-cuts	1	45.45	0.36	0.79

5.4 Chapter Summary and Conclusions

In this chapter the design and development of three different jellyfish robot generations are presented and discussed. The first robot served as a proof of concept and swam vertically at a speed of 2.2 mm/s and consumed 3.2 W of power. This version proved the concept
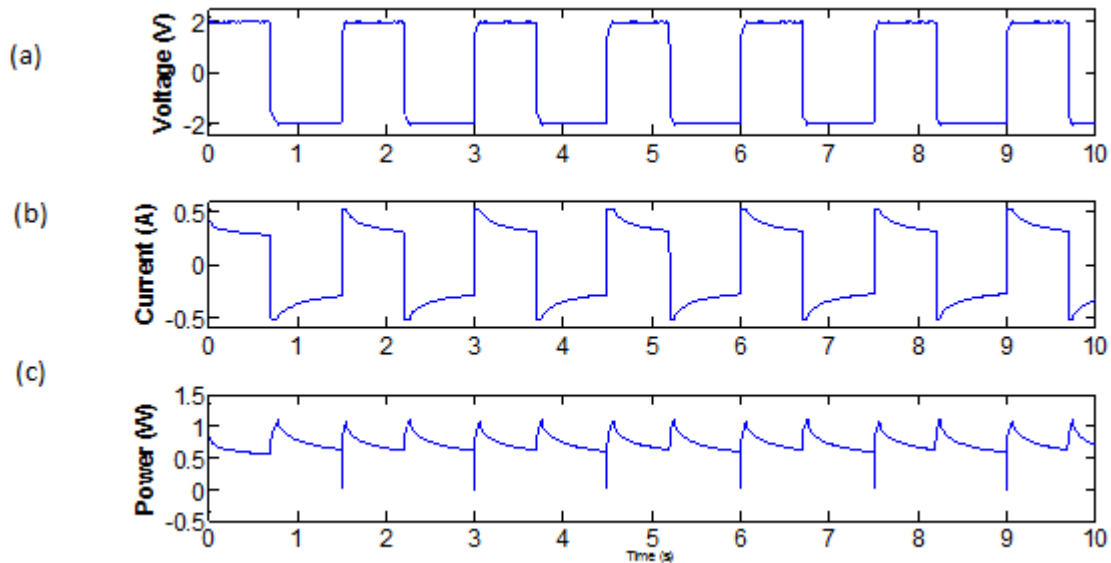
Figure 5.19: (a) The input voltage used to actuate the robotic jellyfish, (b) the current consumption of the robotic jellyfish, and (c) the power consumption of the robotic jellyfish.

of IPMC-based robot and introduced some key parameters that are critical for biomimetic jellyfish robot. The first important parameter is the type, frequency, and duty cycle of the input signal where an unbalanced square wave resulted in higher swimming speeds. The second parameter was the addition of flaps that turned out to be effective in improving the swimming behavior of the robot.

Based on the results of the first generation a second version of the robot was built. This generation mimicked the geometry and swimming style of the *Aurelia aurita* and it swam vertically at an average speed of 1.5 mm/s and consumed 3.5 W pf power. New fabrication techniques were adapted for this design where a polyelfin film was used in order to form a biomimetic bell. These techniques resulted in a light weight vehicle. However, the bell kinematics did not mimic the natural bell kinematics which resulted in unneeded bell deformation and thus more power consumption.
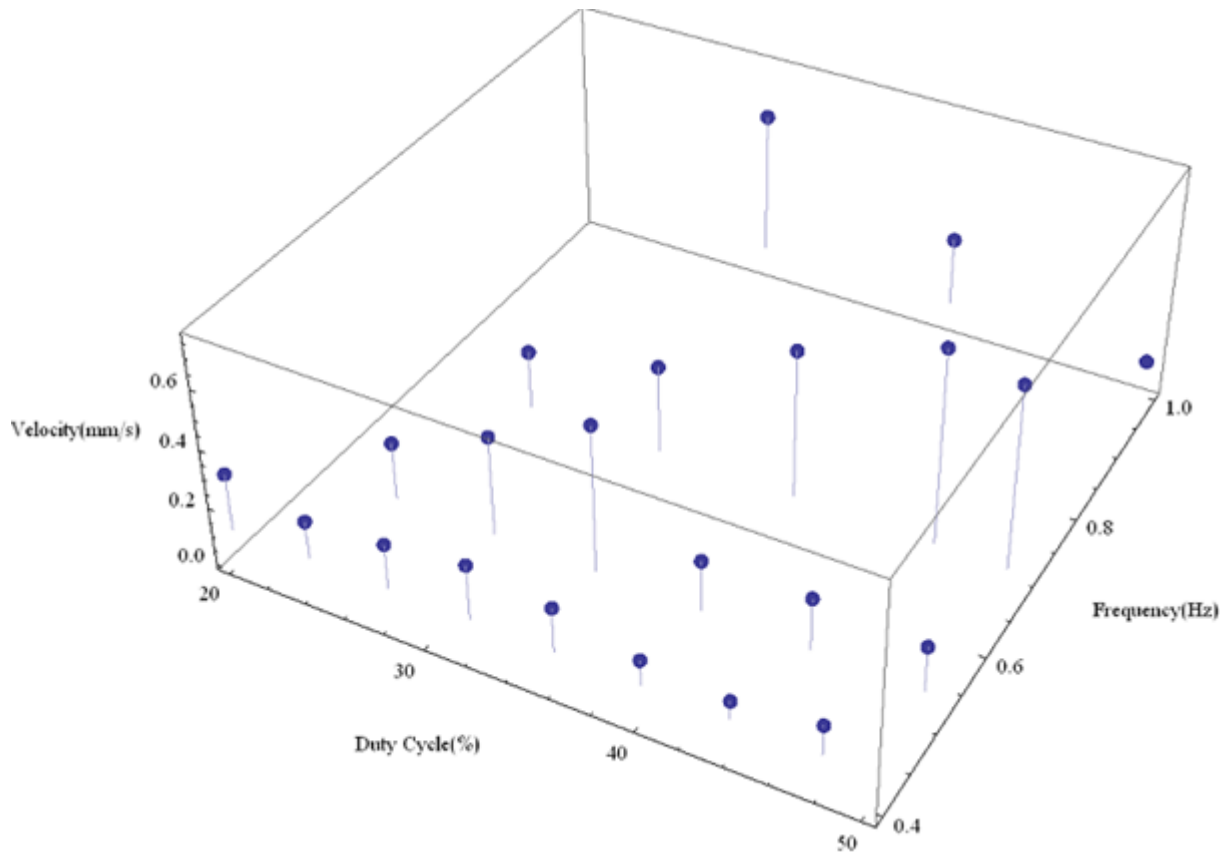
Figure 5.20: A 3D plot showing the velocity of the jellyfish with 4 actuators used in function of frequency and duty cycle, the velocities are in mm/s.

The third and last generation mimicked the geometry, swimming style, and bell kinematics of the *Aequorea victoria*. This robot swam vertically at a speed of 1.5 mm/s and consumed 1.1 W of power when eight actuators were used while it swam at 0.77 mm/s and consumed 0.7 W when four actuators were used. In this design smaller actuators compared to the ones used in previous generations were used due to mimicking the natural bell kinematics by shifting the position of the actuator from the central hub.

Finally, Figure 5.22 show a summary of the three designs. These designs represent a basic study on a IPMC-based biomimetic jellyfish robot. They represent a road map for a more optimized and effective design since the key parameters were identified and can be targeted
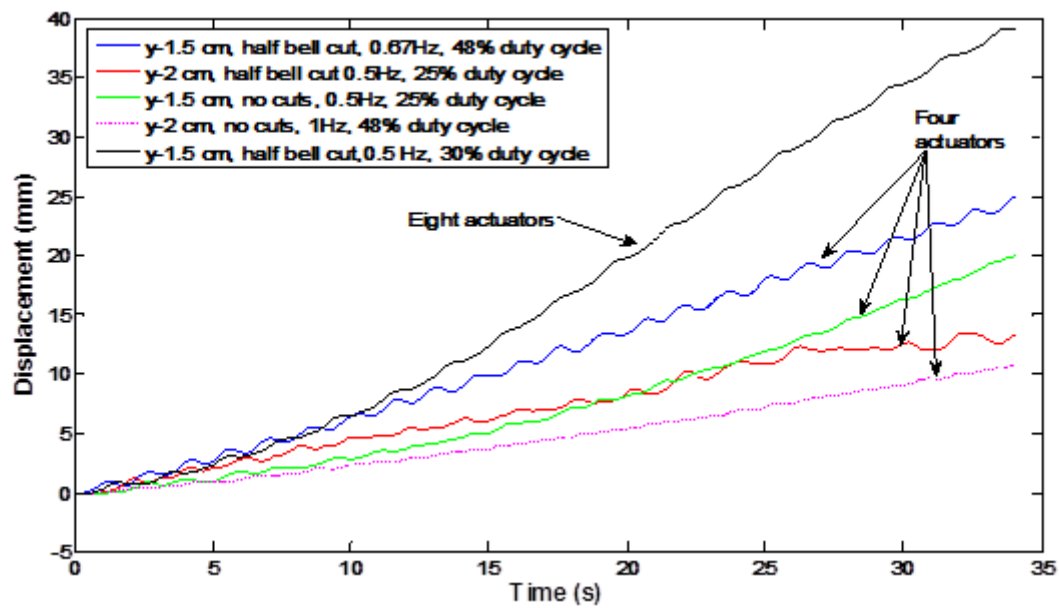
Figure 5.21: The vertical displacement of the jellyfish for different configuration using 4 actuators and 8 actuators.

for any further study.
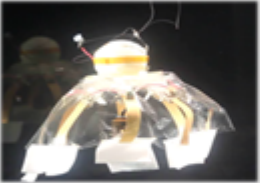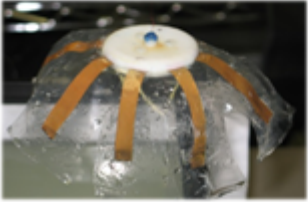
Generation	Speed (mm/s)	Mean power (W)	Notes
	2.1	3.2	• Proof of concept • Non-biomimetic • Flaps increased speed by factor of 3
	1.5	3.5	• Mimics the geometry of the Aurelia aurita • Uniform non-biomimetic bell deformation • No optimization of power
	1.5	1.1	• Mimics the geometry and swimming style of the Aequorea victoria • Bio-inspired bell kinematics • Power reduction due to reduction of the actuators' size • Ability to use less number of actuators

Figure 5.22: A summary of the average swimming speed and power consumption of the three robot generations built in addition to key facts related to each design.

Chapter 6

Summary and Conclusions

In this chapter a brief summary of the thesis is provided. The contributions to the field are presented and major conclusions are drawn. Finally, recommendations for future work are provided.

6.1 Thesis Summary

In this thesis we have designed, developed, and characterized a novel biomimetic robotic jellyfish that uses ionic polymer metal composites actuators. The final design mimics the *Aequorea victoria* jellyfish species, and swam vertically at a speed of 1.5 mm/s and consumed around 1 W of power when eight actuators were used. This design was the result of several initial attempts that helped in understanding the key parameters to a biomimetic robot design.

The initial motivation of this project comes from the interesting properties of the ionic

polymer metal composites especially their ability to exhibit large deformations when a low input voltage is applied. These properties made of the IPMCs strong candidates to replace the SMA actuators used by Villanueva et al in their design of a biomimetic jellyfish robot. The Direct Assembly Process developed by Akle et al was used to fabricate the water based IPMC actuators. This method was optimized for making dry actuators but not the water based ones. Therefore, the electrode structure and chemical composition of the actuator's electrodes were preliminary optimized. The maximum strain percentage achieved was 0.7% in water for an actuation frequency of 0.5 Hz. The actuators were fully characterized and understood. However, the IPMC actuators have two limiting properties that are critical to our design. IPMCs are soft materials and known for a slow response rate since the deformation is due to ion motion through the cluster of the polymer.

In order to overcome these properties different jellyfish species were investigated.The goal is to attain a species that can serve as a system model and fits the mechanical properties of the IPMC actuators. Specifically, we looked for species that achieve small deformations during the contraction cycle i.e. small fineness ratio ranges, and low swimming frequencies. The results proved that *Aequorea victoria* has the smallest fineness ratio and a reasonable swimming frequency of 1.1 Hz. Further comparative studies were conducted between the *Aequorea victoria* and the *Aurelia aurita* which was adapted as a model system for other groups and initially for this project.

Three robot generations were built. The first served as a proof of concept and it swam vertically at 2 mm/s. This version didn't mimic a specific medusa for simplicity, however, it proved that IPMCs can work as actuators for an underwater vehicles. It was learned from this trial the importance of the input signal frequency and duty cycle as well as the importance of the flaps implemented at the margin of the bell. The second generation mimicked the geometry and swimming style of the *Aurelia aurita*, this version swam at a speed of 1.5

mm/s and consumed 3.5 W of power. From this trial it was learned that the geometry of the jellyfish affects the performance of the jellyfish robot. Finally, the final version mimicked the *Aequorea victoria* species and swam vertically at a speed of 1.5 mm/s and consumed 1.1 W of power when eight actuators are used. The same robot swam at a speed of 0.77 mm/s and consumed 0.7 W of power when four actuators are used.

6.2   Conclusions

Ionic polymer metal composites are used as actuators for a biomimetic robotic jellyfish. The limiting properties of IPMCs in this project's case i.e. softness and slow response rate were overcome through two main approaches. First by conducting preliminary optimization studies on the high surface area metal electrodes and second by finding a jellyfish species which properties fits the properties of the actuators. The *Aequorea victoria* was adapted as a model system based on its shape, small fineness ratio range, and slow swimming frequency. The resulting robot swam vertically at a swimming speed of 1.5 mm/s and consumed 1 W of power when eight actuators were used. When four actuators were used the robot swam at 0.77 mm/s and consumed 0.7 W of power. Throughout the research work done on this project it was learned that the input signal amplitude, frequency, and duty cycle affect the swimming speed of the jellyfish robot. On the other hand the addition of flaps and the introduction of cuts to the bell proved to increase the swimming speed of the robot. Finally, this design can be further optimized and studied based on the key parameters that were defined earlier in the thesis.

6.3   Contributions

This thesis has three major contributions to the field of ionic polymer metal composites and biomimetic robotics. These contributions include enhancing the performance of the ionic polymer metal composites, providing basic tools to the fabrication and characterization of biomimetic robotics, and highlighting key parameters that can be later targeted in order to optimize the jellyfish robot. The following is a list of these contributions:

- The first major contribution is the optimization of the water-based ionic polymer metal composites using the Direct Assembly Process (DAP). The achieved percent strain was 0.7% in water for a actuation frequency of 0.5 Hz.

- The second contribution is the development of a fabrication process which allows the manufacturing of biomimetic robots. These techniques allow low power lightweight designs especially the ones that need special shaping based on the biomimetic principles obtained from natural jellyfish..

- Finally, a novel low power biomimetic jellyfish robot was designed and built that utilized IPMCs as the actuation mechanism. Key parameters were identified in order to optimize the design and achieve higher swimming speeds at low power consumption.

6.4   Future Work

Three main recommendations for future works are presented in this section.

- The first recommendation is to further optimize the DAP process for manufacturing water-based ionic polymer metal composites. Improving these actuators by increasing

the strain percentage and rate have a direct impact on the swimming performance of the robot since the biological swimming frequency can be achieved. Another property to optimize is the softness of the material in order to achieve more robust designs.

- A second idea is to better mimic the bell kinematics of the natural jellyfish. This can be done by using patterned actuators and by better locate the position of the actuators. This can result in using smaller actuators and thus reduce the power consumption.

- Since the ionic polymer metal composite act like capacitors at specific frequency the stored current in the actuators can be restored and used to power back the robot. This will definitely lead to more power reduction.

- Finally, study more jellyfish species in order to probably find a better match to the properties of the IPMC actuators. Also consider design robots at smaller scale which might be more beneficial.

Bibliography

[1] B. A. Seibel and J. C. Drazen, "The rate of metabolism in marine animals: environmental constraints, ecological demands and energetic opportunities," *Philosophical Transactions of the Royal Society B: Biological Sciences* **362**(1487), pp. 2061–2078, 2007.

[2] S. P. A. Villanueva, C. Smith, "Biomimetic robotic jellyfish (robojelly)," *Currently unpublished* .

[3] B. Akle, J. Najem, D. Leo, and J. Blottman, "Design and development of bio-inspired underwater jellyfish like robot using ionic polymer metal composite (ipmc) actuators," **7976**, p. 797624, SPIE.

[4] J. Najem, "Design and development of a biomimetic jellyfish robot that features ionic polymer metal composites actuators," *Proceedings of SMASIS, Conference on Smart Materials Adaptive Structures and Intelligent Systems* , 2011.

[5] R. L. Wernli, "Auvs-a technology whose time has come," in *Underwater Technology, 2002. Proceedings of the 2002 International Symposium on*, pp. 309–314.

[6] G. N. Roberts, R. Sutton, and E. Institution of Electrical, *Advances in unmanned marine vehicles*, Institution of Electrical Engineers, London, 2006.

[7] S. E. Showalter, "The law governing autonomous undersea vehicles: what an operator needs to know," in *OCEANS, 2005. Proceedings of MTS/IEEE*, pp. 52–54 Vol. 1.

[8] S. National Research Council . Committee on Future Needs in Deep Submergence, *Future needs in deep submergence science : occupied and unoccupied vehicles in basic ocean research*, National Academies Press, Washington, D.C., 2004. (U.S.).

[9] J. International Symposium on Underwater Technology Tokyo, IEEE, 2000.

[10] N. Franceschini, F. Ruffier, and J. Serres, "A bio-inspired flying robot sheds light on insect piloting abilities," *Current Biology* **17**(4), pp. 329–335, 2007.

[11] P. Leito, *A Bio-Inspired Solution for Manufacturing Control Systems*, vol. 266 of *IFIP International Federation for Information Processing*, pp. 303–314. Springer Boston, 2008.

[12] S. P. Colin, "Morphology, swimming performance and propulsive mode of six co-occurring hydromedusae," *Journal of experimental biology* **205**(3), p. 427, 2002.

[13] "Mechanics and energetics of medusan jet propulsion," *Canadian Journal of Zoology* **61**(6), pp. 1406–1420, 1983.

[14] J. H. Costello, "Kinematic comparison of bell contraction by four species of hydromedusae," *Scientia marina* **64**(s1), p. 47, 2000.

[15] S.-W. Yeom, "A biomimetic jellyfish robot based on ionic polymer metal composite actuators," *Smart materials and structures* **18**(8), p. 085002, 2009.

[16] *Undersea Vehicles and National Needs*, National Academy Press, 1996. Accession Number: 1204. Publication Type: eBook. Language: English.

[17] R. Compton-Hall, "The submarine pioneers," *Recherche (Paris. 1970)* **67**, p. 02, 1999.

[18] M. C. Link, *Windows in the sea*, Smithsonian Institution Press; [distributed by G. Braziller], Washington, 1973.

[19] M. Shahinpoor, "Ionic polymer-metal composites (ipmcs) as biomimetic sensors, actuators and artificial muscles - a review," *Smart materials and structures* **7**(6), pp. R15–R30, 1998.

[20] B. J. Akle, D. J. Leo, M. A. Hickner, and J. E. McGrath, "Correlation of capacitance and actuation in ionomeric polymer transducers," *Journal of Materials Science* **40**(14), pp. 3715–3724, 2005.

[21] B. Akle, M. Bennett, D. Leo, K. Wiles, and J. McGrath, "Direct assembly process: a novel fabrication technique for large strain ionic polymer transducers," *Journal of Materials Science* **42**(16), pp. 7031–7041, 2007.

[22] K. J. Kim, "Ionic polymer metal composites: Ii. manufacturing techniques," *Smart materials and structures* **12**(1), pp. 65–79, 2003.

[23] Y. Bar-Cohen, "Characterization of the electromechanical properties of eap materials," *Proceedings of SPIE, the international society for optical engineering* **4329**, p. 319, 2001.

[24] B. Akle, "Development and modeling of novel extensional ionic polymer transducers," *Proceedings of SPIE, the international society for optical engineering* **6524**, pp. 652411–652411–8, 2007.

[25] J. H. Costello and S. P. Colin, "Morphology, fluid motion and predation by the scyphomedusa lt;igt;aurelia auritalt;/igt," *Marine Biology* **121**(2), pp. 327–334, 1994.

[26] J. H. Costello, S. P. Colin, and J. O. Dabiri, "Medusan morphospace: phylogenetic constraints, biomechanical solutions, and ecological consequences," *Invertebrate Biology* **127**(3), pp. 265–290, 2008.

[27] M. Shahinpoor, "Ionic polymerconductor composites as biomimetic sensors, robotic actuators and artificial musclesa review," *Electrochimica Acta* **48**(1416), pp. 2343–2353, 2003.

[28] M. D. Bennett, D. J. Leo, G. L. Wilkes, F. L. Beyer, and T. W. Pechar, "A model of charge transport and electromechanical transduction in ionic liquid-swollen nafion membranes," *Polymer* **47**(19), pp. 6782–6796, 2006.

[29] K. Oguro, "Polymer electrolyte actuator with gold electrodes," *Proceedings of SPIE, the international society for optical engineering* **3669**, pp. 64–71, 1999.

[30] R. K. Roy, *A primer on the Taguchi method*, Society of Manufacturing Engineers, Dearborn, MI, 2010.

[31] S. Nemat-Nasser, "Micromechanics of actuation of ionic polymer-metal composites," *Journal of applied physics* **92**(5), p. 2899, 2002.

[32] D.-H. Kim, J. Song, W. M. Choi, H.-S. Kim, R.-H. Kim, Z. Liu, Y. Y. Huang, K.-C. Hwang, Y.-w. Zhang, and J. A. Rogers, "Materials and noncoplanar mesh designs for integrated circuits with linear elastic responses to extreme mechanical deformations," *Proceedings of the National Academy of Sciences* **105**(48), pp. 18675–18680, 2008.

[33] B. J. Akle, "Single-walled carbon nanotubes – ionic polymer electroactive hybrid transducers," *Journal of intelligent material systems and structures* **19**(8), pp. 905–915, 2007.

[34] D. J. Williams and M. Shah, "A fast algorithm for active contours and curvature estimation," *CVGIP: Image Understanding* **55**(1), pp. 14–26, 1992.